Review

Not peer-reviewed version

Digital Image Correlation Technique for Laboratory Structural Tests and Applications: A Systematic Literature Review

Mohammed Abbas Mousa *, Mustafasanie M Yussof, Thulfiqar Hussein, Lateef Assi, SeyedAli Ghahari

Posted Date: 25 September 2023

doi: 10.20944/preprints202309.1590.v1

Keywords: Keywords: Digital Image Correlation; Surface displacements; Structural monitoring; Full-scale test design

Review

Digital Image Correlation Technique for Laboratory Structural Tests and Applications: A Systematic Literature Review

Mohammed Abbas Mousa [1,2], Mustafasanie M. Yussof [2], Thulfiqar S. Hussein [1,3], Lateef N. Assi [4] and Seyed Ali Ghahari [5]

[1] Department of Roads and Transportation, University of Al-Qadisiyah, Al Diwaniyah 58002, Iraq
[2] Department of Civil Engineering, Engineering Campus, Universiti Sains Malaysia, Nibong Tebal 14300, Malaysia
[3] Faculty of Civil Engineering, Universiti Teknologi Malaysia, 81310 UTM Skudai, Johor, Malaysia
[4] Terracon Consultants Inc, 9522 E 47th Pl, Tulsa, OK 74145, USA
[5] Department of Civil Engineering, Purdue University, West Lafayette, IN 47907, USA

Abstract: Digital Image Correlation (DIC) is an optical technique used to measure surface displacements and strains in materials and structures. This technique has demonstrated significant utility in structural examination and monitoring. This manuscript offers a comprehensive review of contemporary research and applications that have leveraged the DIC technique in laboratory-based structural tests. The reviewed works encompass a broad spectrum of structural components, such as concrete beams, columns, pillars, masonry walls, infills, composite materials, structural joints, steel beams, slabs, and other structural elements. These investigations have underscored the efficacy of DIC as a metrological instrument for precise quantification of surface deformation and strain in these structural components. Moreover, the constraints of the DIC technique have been highlighted, especially in scenarios involving extensive or complex test configurations. Notwithstanding these constraints, the DIC methodology has validated its effectiveness as a strain measurement instrument, offering numerous benefits such as non-invasive operation, full-field measurement capability, high precision, real-time surveillance, and compatibility with integration into other measurement instruments and methodologies.

Keywords: digital image correlation; surface displacements; structural monitoring; full-scale test design

1. Introduction

In recent years, the evaluation and monitoring of material behaviour and structural performance have become critical aspects of civil engineering research. Laboratory studies in civil engineering often entail the experimental investigation of materials, structural elements, and scale models to understand and predict their performance under various conditions. For these laboratory studies, precise measurement techniques are imperative as they provide critical data that can inform the design, construction, and maintenance of infrastructure. Digital Image Correlation (DIC) is a modern optical method that uses feature tracking and image registration to measure displacement and strain over the whole field of the material or structural elements. Traditional measurement techniques often involve contact with the specimen and may be intrusive or limited in resolution. In contrast, DIC offers high spatial resolution and the capability to capture full-field data, making it highly advantageous for various applications.

Since its early development in the eighties, the DIC methods found various venues of applications in many fields, such as solid mechanics, materials, structures, biology, and others (Chu et al., 1982; Peters & Ranson, 1982). In civil engineering tests, DIC is instrumental in analysing complex phenomena such as crack propagation, deformation under loading, and strain distribution in a non-destructive manner. The DIC's full-field and non-contact characteristics encouraged its use in civil engineering tests and applications as a deformation measuring tool. Though DIC has been employed in a range of studies, there is a vast and growing body of literature, making it difficult for

 doi:10.20944/preprints202309.1590.v1

practitioners to stay abreast of all developments and applications. Evidence of this spread is expressed in the growing body of scholarly articles exploring the potential of the DIC method in structural and civil engineering. Figure 1 presents the number of published documents in the years between 2000 and 2022 when searching the keywords <DIC> "AND" <Civil> related words retrieved from the Web of Science and Scopus databases. Figure 1 shows the increasing trend in published research over the past 15 years, where at least the number of published research papers between 2010 and 2020 tripled.

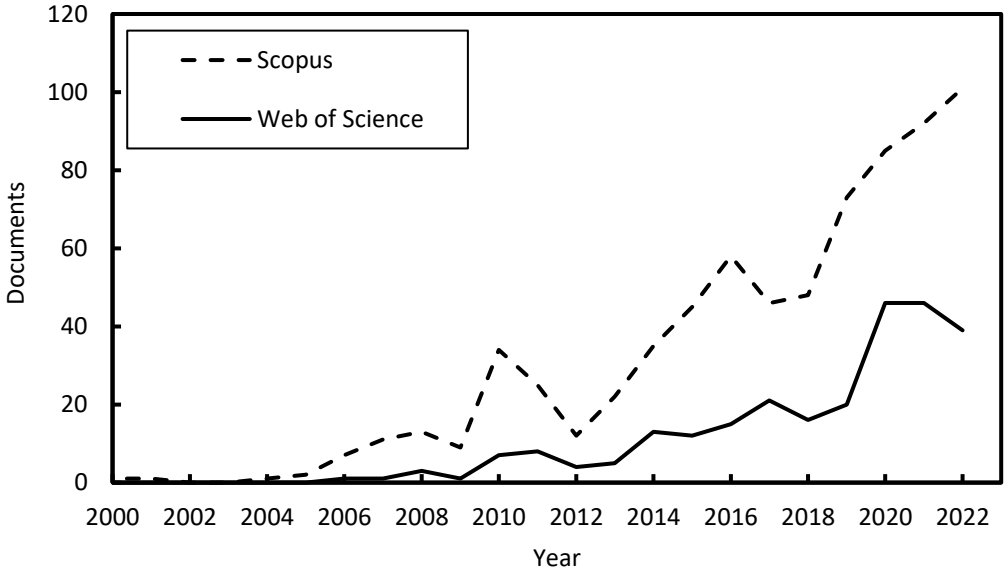

Figure 1. Number of published research articles indexed in Web of Science or Scopus databases using Keywords: ("Digital Image Correlation" OR "DIC") AND ("civil" OR "structure" OR "concrete" OR "beam" OR "steel" OR "concrete beam" OR "steel beam" OR "composite structure" OR "structural joint" OR "column" OR "masonry").

The acceptance and adoption of the DIC technique are credited to two aspects (1) the advancement of optical instruments such as digital cameras and scanners and (2) the rise in computational capabilities of computers. The advancements in digital cameras, such as resolution enhancements, have facilitated the use of the DIC technique for a broader range of applications. For example, the testing of masonry wall and infills need to cover a larger area, which requires a high-resolution camera to provide sufficient spatial resolution. Figure 2 illustrates the progress in resolution improvement of digital cameras and their sensors over the past two decades. The figure showcases the top-performing sensors, whether CCD or CMOS, for each year within this period.

Preprints (www.preprints.org) | NOT PEER-REVIEWED | Posted: 25 September 2023 doi:10.20944/preprints202309.1590.v1

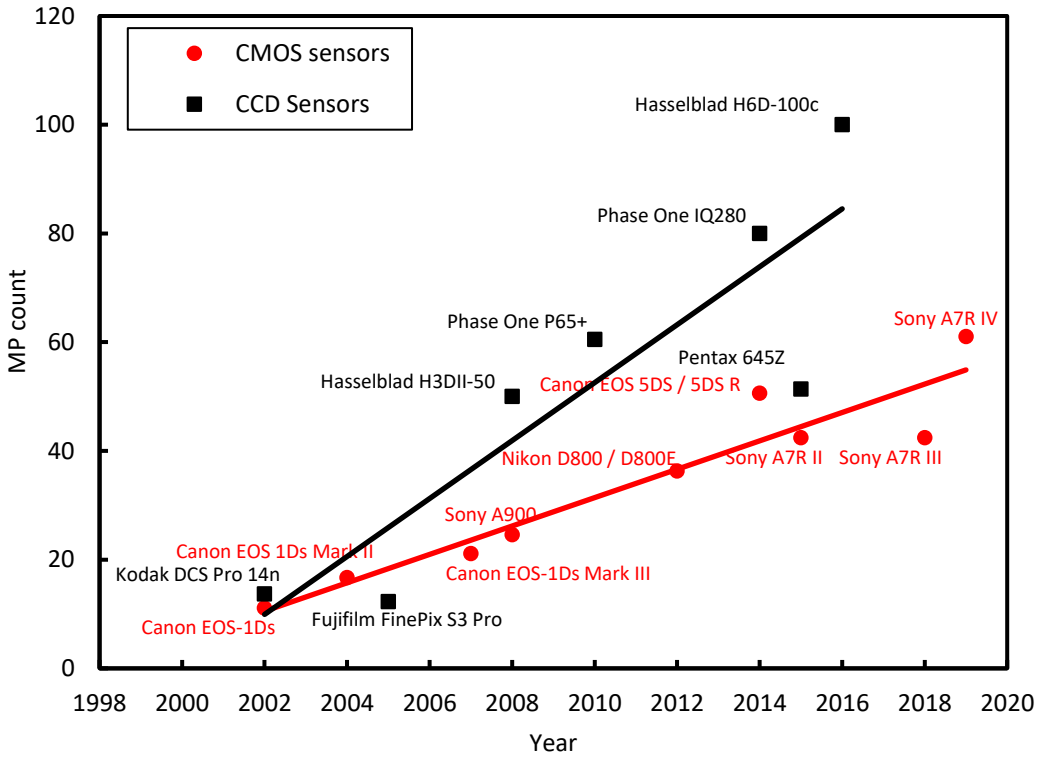

Figure 2. Highest resolution CCD and CMOS cameras for the last 20 years, the sensors count in Megapixels.

Moreover, Figure 3 demonstrates the correlation between camera resolution and the size of the samples examined. It is evident from Figure 3 that as camera resolution improves, there is an observable increase in the size of the areas investigated during DIC structural testing of masonry walls and slabs. It is worth noting that these tests utilizing DIC were not feasible until recently (Bolhassani et al., 2016; Furtado et al., 2015; Ghorbani et al., 2015; Guerrero et al., 2014; Herbert et al., 2011; Hossain et al., 2021; Kumar et al., 2019; Mojsilović & Salmanpour, 2016; Nghiem et al., 2015; Ramos et al., 2015; Salmanpour & Mojsilović, 2013; Torres et al., 2020; Tung et al., 2008).

Preprints (www.preprints.org) | NOT PEER-REVIEWED | Posted: 25 September 2023 doi:10.20944/preprints202309.1590.v1

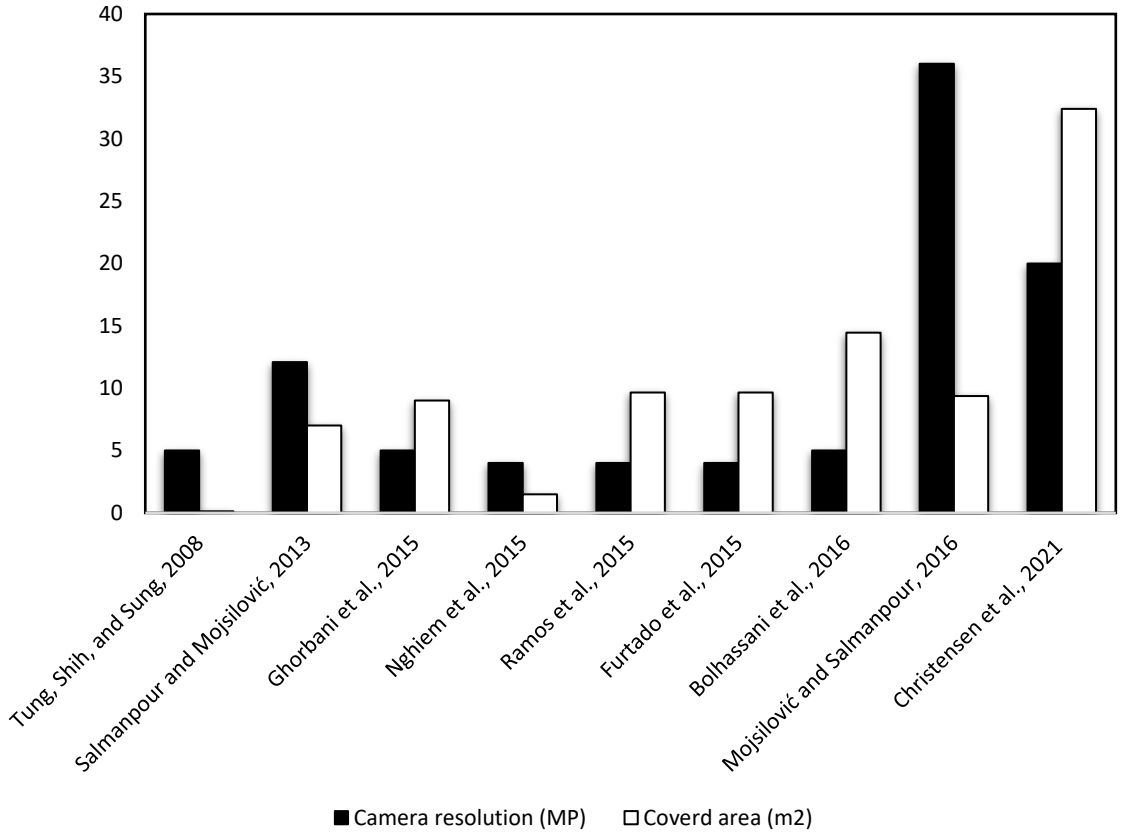

Figure 3. DIC covered areas and camera resolution of masonry and slab tests.

The camera hardware boosting not only helped to utilize the DIC testing of large specimens but also assisted in expanding the usage of the technique for various static and dynamic tests. For example, the progressively increasing cameras frame rates helped to use the DIC for dynamic applications such as determination of the structure natural frequency, seismic response, vibration measurements, and impact tests (Beberniss & Ehrhardt, 2017; Chang & Huang, 2020; Felipe-Sesé et al., 2018; Helfrick et al., 2011; Kalaitzakis et al., 2019; Ngeljaratan & Moustafa, 2017; M. H. Shih et al., 2011; M. Shih & Sung, 2014; Smith et al., 2011; Zona, 2021). In addition, camera portability, such as smartphone cameras has opened new venues for DIC applications in the civil and other fields (Mousa & Yussof, 2021; Tian, Zhang, et al., 2021; Wang et al., 2018a, 2018b; L. Yu et al., 2019, 2021; L. Yu & Lubineau, 2021). Other factors such as sensitivity improvement, noise reduction, automation, and software integration with other techniques such as Acoustic Emissions (AE) (Aggelis et al., 2013; Alam et al., 2014, 2015; Hou et al., 2021; Omondi et al., 2016; Rouchier et al., 2013; Tsangouri et al., 2013), Fiber optics (Bado et al., 2019; Mata-Falcón et al., 2020; Mehdi Mirzazadeh & Green, 2018), and the recent Artificial Intelligence (AI-DIC) and machine learning (ML-DIC) combining (Boukhtache et al., 2020; Miikki et al., 2021; Słoński & Tekieli, 2020; Ziaja et al., 2020) all helped to expand the DIC usage in the civil engineering lab applications. Thus, the DIC applications in the civil engineering field offer great potential due to their non-contact, full-field, high accuracy, versatility, and real-time monitoring.

The purpose of this paper is to present a comprehensive review of the uses of Digital Image Correlation (DIC) in civil engineering laboratory experiments. The paper aims to critically analyse the advantages and limitations of DIC and explore potential future directions. It begins with an introductory overview of DIC, followed by a detailed discussion of its applications in various laboratory civil engineering experiments. These experiments include testing concrete beams, columns, pillars, masonry walls, infills, composite materials, structural joints, steel beams, slabs, and other structural members. Additionally, the paper highlights the limitations of DIC in tests involving

 doi:10.20944/preprints202309.1590.v1

large or complex setups. A summary of the reviewed works is presented in a table format, and the paper concludes with an insightful synthesis of the potential of DIC as a metrological tool for measuring surface deformation and strain in structural members.

2. Laboratory Structural Tests and Applications Using DIC

The DIC is applied by researchers in the laboratory to measure surface deformation and strain of various structural components, as shown in Table 1.

Table 1. A summary of recent laboratory Digital Image Correlation (DIC) research studies conducted in the field of civil engineering testing.

No.	Structural Element	Authors
1	Concrete beams	Ferreira et al. (2011) Destrebecq et al. (2011) Dutton et al. (2014) Gencturk et al. (2014) Alam et al. (2015) Hamrat et al. (2016) Hoult et al. (2016) Omondi et al. (2016) Ruocci et al. (2016) Daghash & Ozbulut (2017) Gali & Subramaniam (2017) Pohoryles et al. (2017) Suryanto et al. (2017) Kearsley & Jacobsz (2018) Mehdi Mirzazadeh & Green (2018) Ghahremannejad et al. (2018) Murali Krishna et al. (2019) Słoński & Tekieli (2020) Zhou et al. (2021) Hou et al. (2021) Enfedaque et al. (2022) Dai & Li (2022) Aryanto et al. (2023) Becks et al. (2023)
2	Columns and pillars	Tung et al. (2014) Shih & Sung (2014) Dai et al. (2017) Demchyna et al. (2019), (2020) Chang & Huang (2020) Fallah Pour et al. (2020) Al-Kamaki (2021) Dai & Li (2022)

 doi:10.20944/preprints202309.1590.v1

		Li et al. (2022) Sun et al. (2023) Allain et al. (2023)
3	Masonry and infills	Tung et al. (2008) Herbert et al. (2011) Salmanpour & Mojsilović (2013) Ghiassi et al. (2013) Guerrero et al. (2014) Furtado et al. (2015) Ghorbani et al. (2015) Nghiem et al. (2015) Ramos et al. (2015) Bolhassani et al. (2016) Mojsilović & Salmanpour, (2016) Kumar et al. (2019) Torres et al. (2020) Hossain et al. (2021) Howlader et al. (2021)
4	Structural joints	Sozen & Guler (2011) Desai (2016) Biscaia et al. (2018) Winkler et al. (2018) Peng et al. (2018) Gorman & Thouless (2019) Sun & Blackman (2020) Chang & Huang (2020) Ziaja et al. (2020) Kim et al. (2021) Paliwal & Ramji (2022) Wani et al. (2022) Xu et al. (2022)
5	Composites	Arora et al. (2011) Ghiassi et al. (2013) Gholizadeh (2016) Pisonero et al. (2017) Dai et al. (2017) del Rey Castillo et al. (2019) Fallah Pour et al. (2020) Janeliukstis & Chen (2021) Spencer et al. (2021) Lim et al. (2022)

Preprints (www.preprints.org) | NOT PEER-REVIEWED | Posted: 25 September 2023 doi:10.20944/preprints202309.1590.v1

6	Steel beams	Peddle et al. (2011) Yoneyama & Ueda (2012) Dutton et al. (2014) Shih & Sung (2014) Yu & Wu (2017) Beberniss & Ehrhardt (2017) Gorman & Thouless (2019) Tian, Zhao et al. (2021)
7	Other members	Beberniss & Ehrhardt (2017) Al-Mosawe et al. (2018) Tehrani et al. (2020) Sharafisafa et al. (2020) Christensen et al. (2021) Miikki et al. (2021) Zhang et al. (2021) Shuai et al. (2022) Thériault et al. (2022)

2.1. Concrete Beams

Concrete beams come in various sizes and configurations and are one of the most lab-tested components using the DIC technique. Gencturk et al. (Gencturk et al., 2014) reported the DIC's advantages and limitations after testing a full-scale prestressed concrete structure. The authors used a stereo 3D-DIC for full-field displacement and strain measurements in conjunction with the conventional displacement transducers. The prestressed I-shaped beam was tested under an ultimate load till failure. It is shown that DIC provided very precise and detailed in and out-of-displacement and strains that were impossible to get with the conventional measuring methods. However, light sensitivity, measuring surface preparations, data loss due to speckle damage following concrete spalling, and the inability of the DIC algorithm to detect and measure crack width were all listed as limitations when utilising the DIC to test the concrete beams (Gencturk et al., 2014).

Alam et al. (2014) applied Acoustic Emission (AE) besides the DIC to identify the parameters of the fractures, such as fracture zone size, crack openings, and the crack tip (Alam et al., 2014, 2015). The author analysed geometrically scaled concrete beams to identify and visualise how cracks initiate and form in concrete. It concluded that combining both techniques provides an efficient and effective tool for fracture and cracking in concrete (Alam et al., 2014, 2015). Similarly, the AE was also used with DIC to investigate the early damage in old-aged RC beams (Hou et al., 2021). The investigation proposed combining AE and DIC to verify the damage where AE delivers an accurate indication of the crack opening and the DIC provides strain, crack pattern distribution, and local and global deformation of the beam. It highlighted that DIC and AE are suitable for damage detection in existing concrete structures (Hou et al., 2021). Similar investigation combining the DIC and AE to identify damage and cracking behaviour in prestressed concrete sleepers of railway structures (Omondi et al., 2016).

DIC was also implemented for crack assessment in large reinforced concrete beams and walls (Ruocci et al., 2016). The author developed a post-processing approach to cope with full-field DIC measurement noise. The suggested approach is validated by testing full-scale and 1/3-scaled reinforced concrete beams under four-point bending. The noise filtering strategy was proven effective and provided accurate estimations such as in-plane displacement and strain fields when post-processing the DIC data. The crack widths and patterns were also identified and measured precisely using the suggested approach (Ruocci et al., 2016).

For characterisation of the shear behaviour of fiber-reinforced concrete beams, Gali & Subramaniam (2017) utilised the DIC to monitor full-field displacement and shear cracks. The tested beams have 125mm x 250mm x 1500mm-(W x D x L), respectively, with 0.5% in volume of 60mm x 0.75mm hooked end steel fibers. The DIC test images were captured with a 5MP resolution camera sensor placed at 1m from the specimens to provide 7-10 pixels per mm. The DIC random error was low after calibration in the range of 0.02 pixels (~0.002 mm). The DIC process was analysed using VIC-2D software to identify and understand the horizontal displacement and shear crack openings using 80 x 80 pixels subsets (Solutions, 2017). It was concluded that using the DIC enabled the tracking of the changes in material behaviour across the crack after the formation of the shear cracks (Gali & Subramaniam, 2017).

Suryanto et al. (2017) investigated the shear behaviour when they used the DIC to map the cracks on shear-critical RC beams. Three RC beams were tested, one control and two others with stirrup shear reinforcements of 0.4 and 1.1 percent. The study investigated the spacing influence on the failure mode, ductility, and overall strength. Open-source DIC software is used to analyse images captured during the four-point bending load (Blaber et al., 2015). The study offered clearer insight into the longitudinal strain fields and post-cracking response to track crack development using the DIC full-field deformation maps (Suryanto et al., 2017).

Daghash & Ozbulut (2017) investigated the flexural response of RC beams reinforced with near-surface-mounted NSM Fibre-Reinforced Polymers (FRP). Five RC beam specimens having a 2.1m were prepared and tested under four-point bending monotonic loading. The tests provided a full-field displacement, strain maps, and deflection using the DIC, while the FRP strain response was captured using strain gauges. The DIC determined the constant moment zone of each beam to calculate the mid-span deflection, which enabled plotting the beam's principal strain and crack distribution (Daghash & Ozbulut, 2017).

Ghahremannejad et al. (2018) investigated the cracking behaviour in concrete beams reinforced with 0.5% and 1% by volume of synthetic fibers. The DIC was used to record cracks' widths, locations, and spacing for all specimens tested under four-point bending loading. The results of crack parameters from the DIC were validated while testing a notched (25mm deep, 5mm width) 150 x 150 x 500 mm beam tested under three point-bending. The notch crack opening displacement of the beam was measured using a clip gauge transducer. The gauge and the DIC results showed an agreement (up to a maximum of 10 % difference) (Ghahremannejad et al., 2018).

The continuous development of the DIC technique led some researchers to try easy methods for surface speckling, such as utilising the Quick Response (QR) technology (Murali Krishna et al., 2019). The study used the QR technology as a random speckle pattern to test an (1800 x 150 x 200) mm RC beam under a four-point bending loading (Murali Krishna et al., 2019). The QR speckle was used beside the traditional random speckle pattern for performance comparison and to serve as a means of embedding data in structural components. The DIC was processed using the open-source Ncorr software operated as code within MATLAB R2015a (Blaber et al., 2015). The images were taken using a 24MP Nikon D5200 DSLR camera equipped with a Complementary Metal-Oxide Semiconductor CMOS sensor. The DIC analysis's findings were contrasted with those of the traditional dial gauge and curvature meters. The moment-curvature response using the QR-based speckle compares well with the conventional dial gauge and machine crosshead results. Other works used the DIC for further testing and verification of concrete beams, such as flexural behaviour and cracking process investigation of 25 years old concrete beam (Destrebecq et al., 2011), fracture analysis of glass fiber-reinforced cement (GRC) (Enfedaque et al., 2015), crack width and slip measurements of RC beam (Hoult et al., 2016), flexural behaviour steel of fibre-RC beam (Hamrat et al., 2016), debonding in FRP and Fibre Reinforced Cementitious Matrix FRCM retrofitted RC concrete beams (Pohoryles et al., 2017), surface crack evaluation of RC elements (Słoński & Tekieli, 2020), and polyolefin fiber-reinforced concrete (Enfedaque et al., 2022).

Finally, the limitation of the conventional 3D-DIC has been addressed by (Dai & Li, 2022) by proposing multi-camera MC-DIC for large coral aggregate concrete beams. The suggested DIC setup has overlapping field-of-view from the multiple cameras calibrated and synchronised to provide a

 doi:10.20944/preprints202309.1590.v1

continuous MC-DIC view. The resulting deformation field is consistent with the strain gauge. The results demonstrate that continuous-view MC-DIC is a valid 3D full-field measuring technique.

2.2. Columns and Pillars

Columns are vital structural elements that transfer the weight of the building from its upper stories to its lower stories through compression. As a result, providing a full-field strain and crack monitoring for such elements is crucial, as failure could result in disastrous consequences. The DIC can also be used with other techniques, such as fiber optics sensors, to measure strain behaviour and profile in reinforced concrete elements. For example, (Bado et al., 2019) combined Distributed Optical Fibre Sensors (DOFS) and Digital Image Correlation (DIC) to monitor reinforced concrete tensile members reinforced steel rebars. The DIC was utilised to determine the concrete's external strains, while the DOFs were internally planted on the rebar surface to measure the reinforcement strain. The test configuration was capturing the images for the DIC using a 24MP camera, taking an image every 5 seconds, and then the images were analysed with GOM correlate software (Metrology, 2019). Both techniques' ability and performance were demonstrated for internal and external strain monitoring of the concrete and steel of the RC concrete members. The DIC confirms the strain peak's locations on the rebars by comparing the results from the DOFs with strain distributions on the surface (Bado et al., 2019).

The application of the DIC was not only limited to concrete but was also used for highly brittle materials such as glass columns (Demchyna et al., 2020). The research included testing multilayer glass columns under central axial compression using 2D-DIC for compression deformation measurement. Although the convenience of the DIC approach has been shown, its inefficiency as a reference method for investigating glass columns is due to photo fixation in one plane. As a result, it was recommended to use the 3D-DIC for column elements (Demchyna et al., 2019, 2020).

The axial and lateral ultimate strains of preloaded RC circular columns wrapped with FRP sheets were also investigated and derived based on data provided by the DIC (Al-Kamaki, 2021). The DIC setup was employed using a VIC-3D system to measure the curved surface of the columns. Eighteen columns with a dimension of 0.20m diameter x 0.75m height were prepared, preloaded through heating and cooling (800-1000 C), and then tested under compression loading. The DIC system characterised the columns and the CFRP sheets for deformation and strain. It concluded that using the DIC technique reveals varied strain distribution along the column height, particularly in pre-heated and confined columns. The results emphasise the DIC's values, showing full-field and not-contact boundary-free methods for stain measurement (Al-Kamaki, 2021).

The multiple-camera MC-DIC work proposed by (Y. Dai & Li, 2022) was also implemented on large slenderness ratio (0.10m diameter x 1.80m height) circular columns. The MC-DIC approach was used to record the 360° of circular columns under the axial compression test. In the test, eight industrial cameras with 5MP resolution and 25mm focal length were used to cover the mid-span region of the column, namely, (0.10m x 0.60m). The MC-DIC has successfully reconstructed the 3D shape of the columns, and both axial and lateral displacement were measured and compared with conventional strain gauges. Similar to (Al-Kamaki, 2021) observation, the strain was not evenly distributed along the column's horizontal and vertical axes, especially in the case of lateral displacement where the concave side except larger compressive displacement than the convex side. The strain measurement shows good consistency with the strain gauge data. As a result, the MC-DIC proved reliable and capable of realising continuous full-field measurements of large slenderness ratio structural components.

2.3. Masonry Walls and Infills

Masonry walls are often unreinforced and vulnerable to out-of-plane loading due to their low inertia in that direction. Observing, monitoring, and detecting strain and cracking in such elements is crucial to prevent tipping, infill separation, corner crushing, diagonal cracking, or collapsing. The DIC was thoroughly employed to investigate various physical components such as displacement, strain, joint motion, drift, and surface bonding to composite and other components of the masonry

walls and infills. For example, the full-field measurements of the deformation and the crack mapping of confined masonry walls were investigated by (Ghorbani et al., 2015) using a 3D-DIC setup beside conventional pointwise sensors. The DIC was employed to determine three full-scale walls having dimensions of (2.43m width x 2.49m height x 0.20m thickness) and constructed from hollow concrete masonry units. The 3D-DIC setup faced several challenges, such as high-contrast speckle patterns design and application for large areas of masonry to ensure optimum spatial and measurement resolution balance. The second challenge is the setup calibration to determine the optimum field of view without sacrificing the spatial resolution. The calibration is performed by manipulating the camera focal length, stereo angle, camera spacing, and camera distance. The third challenge is stereovision lens distortion correction, requiring pre-calibrated grid panels with known spacing. As a result, two Charged Couple Device (CCD) 5MP cameras placed over a rigid bar 1.1m spaced apart with 17.6mm focal length were placed at a 6.7m distance from the wall to capture the full-field 3D deformation components. The DIC results of the displacement and the strain maps were evaluated, and an experimental indication of diagonal strut development was presented for the masonry infills. The crack maps were obtained from the 3D-DIC images based on the principal strain maps. The DIC showed a practical approach to hand-marked crack mapping by showing great details of both strains and crack maps (Ghorbani et al., 2015).

Similar work was performed by (Furtado et al., 2015) where 3D-DIC was employed for large masonry specimen monitoring. In conjunction with the Moire fringe projection technique (for comparison), the DIC was utilised to reconstruct the masonry wall rigid body motion, displacement, and strain measurements in both in-plane and out-of-plane directions. The in-plane test using three hydraulic cylinders was performed in a 4.22m × 2.30m masonry wall cased inside an RC frame. Another out-of-plane test was performed on the masonry wall using the DIC with LVDT. The DIC setup includes using two 4.1MP CMOS sensor cameras with 16mmm focal length lenses, while the in-plane test includes using only one camera, 2D-DIC since only in-plane components are involved. The DIC images were analysed using the VIC-3D™ system provided by Correlated Solutions Co. (Solutions, 2017) The 3D-DIC required calibration to measure the intrinsic and extrinsic parameters of the camera. The displacement and strain field values were considered valid after validation with the Moire fringe technique and pointwise measure LVDT tools. The separation between the masonry and RC frame and corner crushing was also identified using the DIC. However, the diagonal cracking could not be identified because of the wall-side plastering. It is also highlighted that the DIC application is advantageous as it provides a full-field, continuous, and easy measuring technique for motion, displacement, strain, and crack mapping. However, the DIC requires a controlled environment for lighting and vibration prevention, requiring trained personnel for operation (Furtado et al., 2015).

The in-plane shear deformation capacity of unreinforced masonry walls was investigated by (Mojsilović & Salmanpour, 2016) by testing ten full-scale masonry walls exposed to in-plane static-cyclic loading. The deformation was measured using pointwise contact LVDT, potentiometers, and the non-contact DIC technique. The DIC setup involved using two DSLR cameras 12MP (70mm focal length and 0.68m spatial resolution) for the preliminary test and 36MP (50mm focal length and 0.58m spatial resolution) for the primary test. The cameras were placed at 5m and 6m for the preliminary and primary tests, respectively. The camera placement at such a considerable distance served two purposes; to provide a large field of view for specimen measurement and to reduce the out-of-plane effect on the in-plane measurement where the camera distance is inversely proportional to the out-of-plane error. The DIC applicability and issues for large deformation measurements were discussed and highlighted. The displacement and strain field of the deformed masonry walls were successfully evaluated and quantified. However, the post-cracking phase was not analysed due to the speckle pattern damage due to the concrete outer shell falling off. It also highlighted that the DIC could not completely replace the conventional measurement system due to its inability to deliver high-frequency and real-time measurements. This issue was successfully treated later when computers' computational and graphic capabilities were improved. For example, (Padmappriya & Sumalatha, 2018; Pan et al., 2016; Pan & Tian, 2016; Tian et al., 2018; Zhou et al., 2021) all successfully applied the

DIC for real-time displacement and strain measurement applications. The findings showed that an in-house designed DIC system based on standard DSLR cameras could measure the whole deformation field with high accuracy and spatial resolution, even for big specimens and complex deformation fields.

The infilled masonry frame structures were critically evaluated by (Guerrero et al., 2014) by testing several infilled and partially infilled frame specimens exposed to cyclic in-plane loading. The DIC was applied for the displacement and strain assessment of the structure under such loading conditions. No information was provided about the DIC and camera specifications. According to the full-field deformation DIC data, two distinct deformation phases are seen in the masonry infill, one during the hardening stage and another entirely different during the softening phase. Using the DIC method proves that Polyakov's approach works, but only during the hardening phase of the loading. During this time, the infill masonry panel can be replaced by compression struts because concentrated strain bands can be seen in the wall while the rest is only slightly deformed. The "strut" inclination is a significant source of difference between the DIC and the models provided in the literature. The study suggested developing a new macro-model that more realistically describes the softening stage based on data provided by the DIC.

Other DIC applications to masonry include but are not limited to uniform and non-uniform lateral loading to scaled masonry panels (Herbert et al., 2011), bonding of FRP-masonry bonding (Ghiassi et al., 2013), FRCM shear behaviour (Tekieli et al., 2017), Semi interlocking masonry walls cyclic loading (Hossain et al., 2021), masonry damage assessment (Bolhassani et al., 2016; Nghiem et al., 2015), and microcrack and strain monitoring of brick walls (Kumar et al., 2019; Torres et al., 2020; Tung et al., 2008).

2.4. Composites Materials

Due to their mechanical characteristics, environmental resistance (particularly in corrosive atmospheres), fatigue performance, and high weight-to-resistance ratio, composite materials are a viable substitute for conventional steel-based systems in civil engineering rehabilitation and reinforcement of structural elements. The characterisation of the composite material requires quantifying the deformation of the composites' components, namely, the matrix and the reinforcement. As a result, the DIC appears to be a promising technique for composite deformation characterisation as it provides a full-field strain and displacement measurement tool. Moreover, the non-contact feature enables the use of the DIC for hard-to-attach specimens; for example, (Lim et al., 2022) used the DIC to characterise six Fibre-Reinforced Polymer (FRP) grids tested with direct tensile loading. The study used an open-source DIC Ncorr software for image analysis (Blaber et al., 2015). The data calculated from the DIC, namely the Young modulus, were compared with the conventional strain gauge. The DIC setup used an 18MP camera CMOS sensor to capture an image every two seconds during the tensile load test. The camera field of view was zoomed in due to the narrow width of the grid to increase the spatial resolution of the image and enhance the strain accuracy. Results from the DIC were consistent with the strain gauges' data, with less than a 5% difference for all specimens. The study recommended only using the linear average value of the Young modulus and did not recommend using the strain map directly from DIC analysis as it showed too many variations. The instantaneous strain variations could be attributed to several factors, such as light fluctuation, bias error, external vibration, and camera movement. Similar to (Lim et al., 2022) study, (Górszczyk & Malicki, 2019) studied the characteristics of geogrids utilised in GRS systems and pavement constructions using the DIC technique. A successful measurement of the deformation of the geosynthetics during a tension test using the wide-width strips method was made possible thanks to the use of the 2D-DIC methodology in lab control conditions. The measurement approach also allows for validating models of geosynthetics created using the Finite Element Method (FEM). In addition, the employed method permits the description of the comprehensive surface characteristics of the geosynthetic tested, allowing the identification of exhausted areas and those outside the base that can affect the strength and displacements of geosynthetics in geosynthetic reinforced structures.

The influence of confinement material on the compressive behaviour and strain distribution of FRP-confined concrete specimens was studied by (Fallah Pour et al., 2020). The experimental investigation involves testing ten confined and unconfined specimens to measure various types of strains. During axial loading, the development of axial, lateral, and Von Mises strains was monitored and investigated, along with the behaviour of post-peak strain softening. The data provided by the DIC were validated with contact measuring equipment, LVDT, and strain gauge. This study's DIC data demonstrated that the shear zone expansion for unconfined concrete is more localised than for the FRP-confined sample. It was also shown that DIC, compared to contact techniques, gives a more accurate assessment of the final state owing to its capability to capture the development of full-field strains.

Other composite testing and characterisation in civil engineering using the DIC include but are not limited to composite additive manufacturing of large-scale composite structures (Spencer et al., 2021), Carbon Fibre Reinforced Polymer CFRP tensile testing (Pisonero et al., 2017), CFRP-steel composite members bond-slip characterisation (Dai et al., 2017), bond-slip modeling (Biscaia et al., 2018), FRP-Masonry bonding investigation (Ghiassi et al., 2013), and composite sandwich structures dynamic response subject to air-blast loading (Arora et al., 2011).

2.5. Structural Joints

Welding and bolts are the most widely used connection tools to join structural steel members due to their flexibility and rigidity. However, thermal and mechanical stresses may occur in the welded or bolted joints during the welding or bolt fabrication. The different properties of the materials may result in heterogeneous mechanical responses surrounding the joint region. Consequently, by providing a full-field deformation map, the DIC may give extensive data and insight into the weld and bolt-steel interface regions. For example, (Peng et al., 2018) used the DIC during the tensile testing to investigate the local constitutive characteristics of a welded steel joint. The study selected a Q345 steel plate of 20mm thickness as a welded joint. The welded steel plates were cut into two tensile specimens with welding in the center. The samples had a cross-section of 25 mm x 20 mm and 100 mm gauge length. The DIC setup included using two cameras to capture the 3D deformation. The cameras were positioned before the samples' mid-section, and images were captured at a 2-fps sampling rate. Two displacement and strain gauges were also used to capture the sample's longitudinal deformation and validate the DIC data. DIC's estimates of displacement and strain were in good agreement with those from the displacement gauge and strain gauge.

Recently, new software techniques integrated into the DIC have emerged, thanks to the advancements in the application of computer sciences in machine learning, image processing, and computer vision. For example, the DIC was coupled with the artificial neural network to detect anomalies such as the loosened bolts in the beam-to-column joints of a double-story steel frame (Ziaja et al., 2020). The study used a single high-speed Phantom camera (model v341) to record the frame vibration at a frequency of 106Hz. The DIC measurements were taken on eight pre-tensioned bolts that are intentionally loosened bolts to detect the connections' anomaly. The results based on the displacement data from the DIC increased the efficiency in detecting the changes, especially when the algorithm is combined with Artificial Neural Network (ANN), providing an error of less than 1% for false alarms.

Similar work was performed by (Wani et al., 2022) to capture the in-plane drift of a five-story steel frame subjected to high-intensity shaking. The high-speed Basler Ace cameras were used to observe the speckle patterns applied at every beam-column joint to capture the global response of the structure. DIC configuration uses a streaming capture technique, which determines video capture frequency using the Nyquist factor and peak resonant frequency. The camera setup was a 2.3MP full high-definition resolution camera with a 16mm focal length recording images at a maximum rate of 162 fps. The results provided by the DIC were compared with responses provided by the wire transducers. The study addresses the limitations of the wired transducers compared to the newly configured streamed DIC. As a result, feedback-based control systems may benefit from combining

streaming DIC with the template matching algorithm since it proved effective in identifying and monitoring various responses.

Other work concerning a steel beam-to-column connection was also investigated (Desai, 2016). The DIC was used to observe the smallest strain measurements in the connection under controlled laboratory conditions. Strains were measured using the DIC method, and their accuracy was evaluated by comparing the results to those obtained using traditional strain gauges. Finally, the smallest strains that could be reliably measured using the DIC method were found. Three steel plate connection specimens were used to connect through sandwiching an 850mm steel cantilever beam prone to a single load at its free end. An array of strain gauges was used besides the DIC for comparison. The DIC images were captured using a Nikon D800 camera having 36MP resolution at a rate of 0.02 fps (an image every 30, 60, 75 seconds, optimum 45 seconds). The camera was placed at a very close distance (7.5 to 20cm, optimum 10 cm) from the connection surface to capture the smallest strain value possible. The strain results from the DIC were determined and can accurately measure compressive strains as low as 0.03%. However, a pronounced difference between the strain values provided by the strain gauges with the DIC was noted. These differences were attributed to various factors such as specimen vibration, camera vibration, and strain gauge calibration errors. The DIC technique for joint observation in the lab testing was investigated and highlighted. However, the study suggested improvement, and more work is needed to successfully apply the DIC for field applications.

In addition, steel is not the only material that makes up the joints. For example, the CFRP laminate hybrid joint was investigated for damage evolution and failure through single-lab direct tensile testing (Paliwal & Ramji, 2022). With the use of the Acoustic Emission AE method for damage evolution capturing, the DIC was used to examine the full-field displacement and strain in simple bonded and bolted joints. Both two (180mm focal length) and three (50mm focal length) dimensional DIC using two Grasshopper CCD cameras at a rate of 5 fps. Numerical modeling was also employed to validate the DIC and AE's experimental data and data provided by wired strain gauges, which were impeded in the bolts.

Other joint-DIC applications include but are not limited to strain distributions in bolted steel elements (Sozen & Guler, 2011), epoxy adhesive joints fracture behaviour characterisation (Kavdir & Aydin, 2019), hybrid bonded-bolted composite joints (Kim et al., 2021), and metal laminate joints (Xu et al., 2022).

2.6. Steel Structures

Steel beams and girders compose essential structural members in bridges and steel structures. As a result, measuring the full-field deformation to understand the structural behaviour, such as strain, deflection, and curvature is essential. For example, the curvature of the steel beam was investigated by (Dutton et al., 2014) using the DIC. The level of accuracy of the DIC curvature measurement technique was investigated by testing a Hollow Structural Section (HSS) steel beam under three-point bending in a controlled laboratory setting. Two Canon T2i cameras with 180mm focal lenses were placed at 1.6m from the beam face to deliver a spatial resolution of 0.036mm/pixel. Three strain gauges were placed at the beam's top and bottom face beside the DIC for further strain monitoring and validation with DIC data. The beam curvature from the DIC showed a similar linear trend and slope with the strain gauges. However, a consistent discrepancy existed between the measured curvature from the DIC and the foil gauges. An initial out-of-plane beam displacement relative to the camera before the first load might explain the offset. Because of this, a second DIC analysis was performed, this time with the averaged picture from the first load stage serving as the reference image to correct for the out-of-plane effect. The modified strain profiles for the chosen gauge lengths provide a decent fit in curvature predictions for the DIC virtual and the physical strain gauges.

DIC is used to analyse an adhesively bonded double-cantilever beam and calculate a cohesive-zone model's traction-separation law (Gorman & Thouless, 2019). DIC is utilised to identify both the cohesive zone and the elastic arms evolve according to loading and the adhesive. The double

cantilever beam was made of 4130 steel sheets having a thickness of 4.8mm and 152mm in length. Two 5MP cameras were synchronised and utilised to provide images for the DIC VIC-2D software (Solutions, 2017). The results from the DIC were utilised for obtaining the traction-separation law through obtaining the loading points rotation and the J-integral. In addition, shear strains and cohesive zone deformation were also explored from the full-field data provided by the DIC. By establishing a correlation between the cohesive-length scale and the growth of the cohesive zone and the root rotation, it was demonstrated that these two features scale in a remarkable way that is in line with the analytical calculations of an elastic foundation model. In summary, the full-field deformation data offered by the DIC provides a better cohesive zone development model.

In addition, experimental tests have been made to assess the applicability of DIC for deflection measurement of large wide flange steel beams (Yoneyama & Ueda, 2012). The beam was made of SS400 steel having 200mm width, 8mm thickness, and 5m long, tested under a three-point bending load. The images were recorded for DIC analysis using a single DSLR camera with an 8MP resolution. A new method was developed for DIC data correction based on camera movement correction by capturing undeformed reference surfaces within the camera field. Thus, the camera was moved and positioned in the same place to verify the applicability of the proposed method. Using displacement transducers, the beam deflection was measured at multiple positions, namely, ¼, ½, and ¾ of the beam length. Then, deflection based on DIC data was extracted, corrected, and compared with the transducers' displacement. The deflection curves after DIC data correction agree well with the deflection from the gauges.

Recently, a new method based on off-axis DIC was proposed by (Tian, Zhao, et al., 2021) by using a video deflectometer beside the DIC camera. The new method calculates all the bridge points of interest with a scale factor based on the assumption of the spatial straight-line fitting. The proposed full-field bridge deflection measurement method was tested by applying a static load on a thin cantilever beam 950mm long to verify the method's accuracy. The distance between the video deflectometer and the steel support beam is one meter. The lens has an 8 mm focal length, and the deflectometer has an 11-degree pitch angle. A set of dial gauges was placed on the new proposed beam at multiple locations for deflection measurement and to verify the new off-axis DIC method. The benefits of the proposed full-field bridge deflection measurement over the traditional single-point measuring method are: Only the distances to the camera are required, and the 2D-DIC analysis is demonstrated to be accurate and efficient. The newly proposed method proved a robust optical tool for bridge deflection measuring. Other DIC applications are the mechanical characterisation of a three-point bending of simply supported a W-steel beam (Peddle et al., 2011) and dynamic analysis and damage detection of multi-story steel frame (Shih & Sung, 2014).

2.7. Slabs and Other Members

Advanced monitoring systems are necessary to identify stop criteria during proof-loading concrete slab bridges. Recently, (Christensen et al., 2021) investigated the standard measuring technique of crack identification and assessment using the 2D DIC technique. The DIC capabilities were explored by testing three Overturned T-beam RC slabs under controlled laboratory conditions. Two of the concrete slabs were stripped from an in situ full-scale Ot-slab bridge having a 9m span and one downscaled slab. Two cameras were used for DIC imaging, one having 20MP placed at 3.8m from the bridge surface. The other camera was placed closer at 2.6m and had an 18.7MP resolution. The concrete slab test setup includes a pin supported from three edges (two short span-1.6m and one long -7.5 m) and one free long edge, and the load actuator was placed in the middle of the long span and 0.5m from the free edge. The test setup consists of LVDT, distance lasers, potentiometers, strain gauges, and 2D-DIC. The DIC data were analysed with GOM correlate software (Metrology, 2019). The crack width measurements were successfully acquired using the 2D-DIC images after out-of-plane movement correction. The load-deflection and crack widths from the DIC agree well with the data provided by pointwise sensors. As a result, the DIC technique seems suitable for identifying stop criteria in the proof-loading of the in-situ bridge section.

 doi:10.20944/preprints202309.1590.v1

In addition, the DIC was also used for various qualitative and quantitative civil engineering tests and applications. For example, the shear push-off testing of seven double-L shape RC specimens was investigated by (Thériault et al., 2022) employing the DIC technique. The crack kinematics was observed using the DIC's full-field strain and displacement data. This research proposes a cheap and easy method to add quantitative measures to regular visual inspections by processing images captured with a portable digital camera using open-source DIC software. Two separate cameras were implemented during the test, one primary having an 18MP and the secondary camera having a 24MP resolution. A fixed rectangular aluminum frame reminiscent of the procedure used by (Pan et al., 2014; Tian et al., 2018; Wittevrongel et al., 2015) was used as a reference for DIC data to compensate for the movements involved during the test. During the test, four camera movement types were considered, (1) camera parallel to the structure shifting, (2) camera movement toward the structure, (3) camera rotation vertically, and (4) camera titling, horizontal rotation. The study concluded that a significant error was observed for the uncorrected DIC measurements attributed to the camera movement. However, the proposed correction enhanced the experiment measurements, where 96 and 99% of the residual errors were within 0.1mm of the corrected slip and crack width, respectively.

3. Summary of the DIC-Civil Engineering Laboratory Tests and Applications

A summary of the reviewed DIC tests and applications is presented in Table 2. Table 2 shows the author's name, year of publication, the specimen type, test method, the measured parameters, and the camera specification such as sensor resolution (Mega Pixel - MP) and measurement resolution ($\frac{Pixel}{mm}$ - px/mm), and the DIC software used for the analysis.

Table 2. Summary of the recent lab DIC applications for civil engineering tests.

1. Concrete Beams			
Author	**Specimen type and test method**	**Measured parameters**	**DIC specifications (Camera resolution, Measurement resolution, DIC software)**
(Destrebecq et al., 2011)	full scale RC beam after 25 years of service in an industrial environment, four-point bending.	Displacement fields. Cracking process.	**1-MP**, **1.38 px/mm**, **SeptD** (Vacher et al., 1999)
(Tsangouri et al., 2013)	Plain concrete prisms 840mm long, 100mm wide, and 100mm high, three-point bending and a crack mouth opening displacement.	To visualize the crack opening and strain monitoring.	**5-MP, 20 px/mm, VIC-2D** (Correlated Solutions, n.d.-a)
(Aggelis et al., 2013)	RC beams with a length of 2.5 m, a distance between the supports of 2.3 m, and a height and width of 0.3 m and 0.2 m respectively. A four-point bending test.	To measure the displacement and deformation fields at the side and the bottom	**Not reported, Not reported, VIC-3D** (Correlated Solutions, n.d.-b)

		surface of the beams.	
(Dutton et al., 2014)	Two different sections and materials, i.e., a steel HSS and a series of RC beams. Three-point bending.	longitudinal strains with the height at a section (curvature).	**18-MP, 27.8 px/mm, GeoPIV** (Stanier et al., 2016; Take, 2015; White et al., 2003)
(Gencturk et al., 2014)	Full-scale deep I-beam prestressed concrete beam, shear capacity test.	In-plane and out-of-plane strains. Tensile and compressive strain locations.	A pair of **12.6-MP, Not reported, GOM 3D** (Metrology, 2019)
(Alam et al., 2014, 2015)	Geometrically scaled concrete beams under bending test.	fracture parameters such as crack openings and fracture zone size	**1.4-MP, 5.5-28.5 px/mm, VIC-2D** (Correlated Solutions, n.d.-a)
(Omondi et al., 2016)	Prestressed concrete sleepers. Three-point Negative bending test.	critical damage areas evolution as a function of loading periods	**5-MP, 7.1 px/mm, VIC-3D** (Correlated Solutions, n.d.-b)
(Ruocci et al., 2016)	RC beams. 1. Full-scale rectangular beams. 2. One-third scaled mock-ups. Four-point bending.	Evolution of the cracks pattern. Crack width, deformation, and strain monitoring.	**12-MP, 2 px/mm, MICMAC** (Pierrot-Deseilligny & Paparoditis, 2006)
(Hoult et al., 2016)	RC beams with both small and large crack slip. Three and four-point bending test.	Crack width and crack slip measurement	**18-MP, 7.5-21 px/mm, GeoPIV** (Stanier et al., 2016; Take, 2015; White et al., 2003)
(Hamrat et al., 2016)	Normal strength, high strength concrete, and high strength fiber concrete. Nine RC beams tested under four-point bending.	Strain, crack detection, development, and width measurements	**Not reported, Not reported, GOM 3D** (Metrology, 2019)
(Pohoryles et al., 2017)	Composite-retrofitted RC beams. Four-point bending.	Strain and displacement monitoring, cracking, and debonding	**5-MP, 4.6 px/mm, DaVis 8.2.1** (GmbH, 2009)

Preprints (www.preprints.org) | NOT PEER-REVIEWED | Posted: 25 September 2023 doi:10.20944/preprints202309.1590.v1

(Gali & Subramaniam, 2017)	RC beams reinforced with steel fibres, the beams have dimensions 1500mm length, 125mm width, and 250mm depth. Four-point test, beams with a shear s/d ratio = 1.8.	Cracks and crack patterns identification. Tracking the response of the concrete across a crack. Horizontal and vertical displacements	**5-MP, 7-10 px/mm, VIC-2D** (Correlated Solutions, n.d.-a)
(Suryanto et al., 2017)	Three RC beams, two with shear and one without shear reinforcement having dimensions 100×150×2000 mm3. Four-point loading test.	Crack mapping. longitudinal strain fields.	**18.4-MP, 4.4 px/mm, Ncorr** (Blaber et al., 2015)
(Daghash & Ozbulut, 2017)	Five RC beams strengthened with NSM-BFRP having length of 2.1m. Four-point bending test.	Full-field strain and displacement contours. Mid-span deflection. Measurement of cracks width.	**5-MP, Not reported, Not reported**
(Ghahremannejad et al., 2018)	Fibre-reinforced concrete beams six 1143 x 229 x 152 mm with and six 507 x 152 x 152 without longitudinal reinforcement. Four-point test.	Cracks kinematics (locations, number, spacing, and width).	**Not reported, Not reported, GOM 2D** (Metrology, 2019)
(Murali Krishna et al., 2019)	A 24 (RCC) beams of size 1800 mm x150 mm x 200 mm.	To obtain the Moment (M) – Curvature (κ) relationships	**24.1-MP, Not reported, Ncorr** (Blaber et al., 2015)
(Słoński & Tekieli, 2020)	Post-tensioned, precast crane runway I-section beams having dimensions of 6 m length and 0.8 m height after more than 50 years of exploitation. Three-point bending test.	Full-field strains. Detecting and locating the cracks on the surface. Combining DIC with R-CNN.	**Not reported, Not reported, µDIC** (Olufsen et al., 2020)
(Domaneschi et al., 2021)	RC beam with 4 x 0.3 x 0.15 m. four-point bending test.	strain field	**Not reported, Not reported, Ncorr** (Blaber et al., 2015)

Preprints (www.preprints.org) | NOT PEER-REVIEWED | Posted: 25 September 2023 doi:10.20944/preprints202309.1590.v1

(Hou et al., 2021)	full-scale RC beam that served for 60 years in an industrial environment, four-point bending test.	Strain, crack pattern and distribution, global and local deformation	**5-MP, 7.7 px/mm, DANTEC Istra 4D** (Nova Instruments, 2016)
(Enfedaque et al., 2022)	polyolefin fibre RC beam. Three-point bending fracture test results.	Crack width. Crack opening displacement plane	**5-MP, 200 px/mm, Not reported**
(Y. Dai & Li, 2022)	Coral aggregate concrete beam having dimensions of 1350 mm x 200mm× 120mm. Four-point bending.	A continuous-view multi-camera DIC to measure continuously the full-surface deformation.	Eight cameras, **5-MP, 290 px/mm, Not reported**
(Aryanto et al., 2023)	Four concrete beams (150 x 150 x 600 mm) tested under four-points bending load.	Displacement fields. Crack propagation.	**18-MP, Not reported, Py2DIC** (Belloni et al., 2019)
(Becks et al., 2023)	An inverted prestressed T-beam with a 1.4m long was tested in four-point bending.	Longitudinal compressive strain profile.	**12-MP, 10 px/mm, GOM 3D** (Metrology, 2019)
2. Columns and pillars			
Author	**Specimen type and test method**	**Measured parameters**	**DIC specifications (Camera resolution, Measurement resolution, DIC software)**
(Demchyna et al., 2019)	Multilayer of glass and polymeric film sheets columns with 1000mm height, 5 x10mm thickness of sheets, and 70mm width. Compression test.	Determining the relative deformation and the strain of the glass.	**18-MP**, **Not reported**, **GOM 2D** (Metrology, 2019)
(Bado et al., 2019)	Three types of RC tie members tested under uniaxial tensile loading where the samples clamped to the testing machine from the reinforcing bars.	To determine the surface displacements and strains of the columns.	**24-MP**, **7.5-10 px/mm**, **GOM 2D** (Metrology, 2019)
(Demchyna et al., 2020)	Glass columns of two series of 70 x 100 and 35 x100 sections	The use of 2D-DIC for glass columns	**18-MP**, **Not reported**,

	both having 1m height. All samples were tested under compression load.	under compression is not possible, because the columns are deformed in the direction of the three axes in space. For the study, it is necessary to use 3D-DIC.	**GOM 2D** (Metrology, 2019)
(Al-Kamaki, 2021)	Pre-loaded RC columns through heating and cooling, then repaired with CFRP sheets. Compressions test.	to determine both latera and axial surface strains of the undamaged and post heated CFRP-confined columns.	**5-MP, 1.1 px/mm, VIC-3D** (Correlated Solutions, n.d.-b)
(Y. Dai & Li, 2022)	Circular timber slender column with 100 mm in diameter and 1800mm height were tested under compression load.	Fully reconstructing the 3D shape of the circular column	Eight cameras, **5-MP, 290 px/mm, Not reported**
(Z. Sun et al., 2023)	A precast concrete column reinforced with steel-FRP composite bars. Six columns (300 x 360 x 1400 mm) were tested under low reversed cyclic loading	Strain distribution. Moment-curvature curves. Plastic hinge region. Rotation calculation.	**Not reported, Not reported, Not reported**
(Allain et al., 2023)	Concrete column under controlled load given vertical stress of 2.4 MPa in compression.	Displacement and strain field.	**12-MP, 22 px/mm, GlobalDIC and 7D** (Vacher et al., 1999)
3. Masonry walls and infills			
Author	**Specimen type and test method**	**Measured parameters**	**DIC specifications (Camera resolution, Measurement resolution, DIC software)**

(Tung et al., 2008)	A 45° brick wall having dimensions of 30 x 40 cm and 150 x 120 cm steel-framed brick wall both tested under compression load.	Displacement and strain measurement. Crack observation	**6.3-MP, 5 px/mm, Not reported**
(Herbert et al., 2011)	1/6th scale masonry wall panels using a centrifuge to correctly model self-weight. A uniform lateral loading using airbag or non-uniform hydraulic loading.	Deflection of the panels. Identification of cracks in the wall panel.	**Not reported, Not reported, Not reported**
(Salmanpour & Mojsilović, 2013)	Eleven full-scale unreinforced masonry walls ranging from (1.5 x1.6 m) to (3.6 x 2.6 m) were subjected to in-plane cyclic loading.	Deformation, strain, and crack distribution.	**12-MP and 36-MP, 1.5 – 1.7 px/mm, VIC-2D** (Correlated Solutions, n.d.-a)
(Guerrero et al., 2014)	One single-bay infill, one single-bay partially infilled frame, Two-bay partially infilled frame, and squat infilled frame. All were subjected to cyclic lateral loading.	Strain fields. Struts inclination.	**Not reported, Not reported, CORRELI-Q4** (Besnard et al., 2006)
(Ghorbani et al., 2015)	Three full-scale masonry walls with dimensions of 2.4 x 2.4 m confined in a RC frame. All specimens were subjected to lateral in-plane cyclic loading.	Drift and diagonal deformation fields. Slip at the interface between the masonry and the concrete tie column.	**5-MP, 0.72 px/mm, VIC-3D** (Correlated Solutions, n.d.-b)
(Nghiem et al., 2015)	a large-scale physical model reproducing both the soil-structure interaction and the masonry structure. Loading is applied by means of ground surface displacement.	Propose a way to quantify DIC measurement errors. Reconstruction of motion Displacement fields. Damage evaluation.	**4-MP, 7 px/mm, VIC-3D** (Correlated Solutions, n.d.-b)
(Ramos et al., 2015)	A full-scale 4.2 x 2.3 m masonry wall confined with RC frame. Two tests were applied, one in-	Displacement and strain fields. Principle strains.	**4-MP, 2 px/mm,**

	plane shear test and quasi-static out-of-plane cyclic test.	Out-of-plane displacement.	**VIC-3D** (Correlated Solutions, n.d.-b)
(Furtado et al., 2015)	A full-scale 4.2 x 2.3 m infilled RC frame subjected to in-plane test. One double leaf-panel.	Diagonal cracking, corner crushing, shear-friction failure.	**4-MP, 2 px/mm, VIC-3D** (Correlated Solutions, n.d.-b)
(Bolhassani et al., 2016)	A full-scale 3.8 x 3.8 m partially grouted masonry shear wall tested under constant vertical compression load and horizontal lateral load using quasi-static displacement procedure.	Crack patterns. Diagonal tension and compression strains. Bed joint shear. Base strain.	**5-MP, 0.5 px/mm, GOM 3D** (Metrology, 2019)
(Mojsilović & Salmanpour, 2016)	Ten full-scale unreinforced masonry walls ranging from (1.5 x1.6 m) to (3.6 x 2.6 m) were subjected to in-plane cyclic loading.	Deformation, strain, and crack distribution.	**12-MP and 36-MP, 1.5 – 1.7 px/mm, VIC-2D** (Correlated Solutions, n.d.-a)
(Kumar et al., 2019)	Brick masonry prisms with dimensions of 520 x 220 x 100 mm tested under uniaxial compressions load.	In-plane strains and displacement.	**12-MP, Not reported, Ncorr** (Blaber et al., 2015)
(Torres et al., 2020)	Six 710x710 mm brick masonry specimens tested under diagonal tension tests to evaluate the shear behaviour.	Identify the strain distribution at the moment of failure. Deformation measurement. Shear modulus.	**24-MP, 100 px/mm GOM 2D** (Metrology, 2019)
(Hossain et al., 2021)	Different types of engineered masonry panels (2 x 2 m) made of semi-interlocking masonry (SIM) units subjected to in-plane cyclic loading.	von Mises strain fields. Joint opening and propagation. Horizontal and vertical displacement.	**8-MP and 36-MP, 7.4 – 21.5 px/mm, VIC-2D** (Correlated Solutions, n.d.-a)
(Xie et al., 2023)	Four full-scale models of masonry infill having (3.1 x 3.0 m) surrounded by RC frame tested against out-of-plane loading.	Full-field out-of-plane deformation and strain concentration analysis.	**12-MP, Not reported, GOM 3D** (Metrology, 2019)

 doi:10.20944/preprints202309.1590.v1

4. Composites materials			
Author	**Specimen type and test method**	**Measured parameters**	**DIC specifications (Camera resolution, Measurement resolution, DIC software)**
(Arora et al., 2011)	GFRP sandwich structure having a speckled target of 1600 x 1300 mm subjected to a blast load.	Deformation monitoring. Failure mechanism.	**Two high-speed cameras of 1000FPS, 1-MP,** **0.787 px/mm,** **GOM 3D** (Metrology, 2019)
(Ghiassi et al., 2013)	FRP-masonry composite, to characterise the bonding interface through tensile and shear tests.	Longitudinal strain distribution in tensile test. Strain distribution along the bonded length in shear test.	**2-MP,** **27 px/mm,** **GOM 2D** (Metrology, 2019)
(Y. T. Dai et al., 2017)	CFRP-steel composite structure with dimensions of 150 x 150 x 500 mm. Shear test to monitor the bond-slip and compression test to monitor the buckling location.	To derive the bond-slip relationship between the CFRP-steel interface. To precisely locate the buckling and delamination of CFRP-steel composite.	**A multi camera system, 4-MP and 5-MP,** **Not reported,** **PMLAB DIC-3D_2014a** (PMLAB, 2014)**.**
(Tekieli et al., 2017)	Bond and tensile tests on composite reinforcements comprising different textiles and matrices.	Damage pattern (crack location and width) . Load transfer mechanism between composite-to-substrate.	**24-MP,** **9 px/mm,** **Two software; CivEng Vision** (Tekieli & Słoński, 2013) **and Ncorr** (Blaber et al., 2015)
(Pisonero et al., 2017)	Several DIC (2D and 3D) methods were employed using tensile tests to characterise 25 CFRP composite specimens.	The Young modulus. The Poisson ratio.	**Two systems:** **2D: 18-MP, 3D: two 18-MP,** **Not reported,**

Preprints (www.preprints.org) | NOT PEER-REVIEWED | Posted: 25 September 2023 doi:10.20944/preprints202309.1590.v1

		Displacement and strain.	**2D: Ncorr** (Blaber et al., 2015) **3D: MultiDIC** (Solav et al., 2018)
(Górszczyk & Malicki, 2019)	Twenty specimens of 20 x 30 cm of Geosynthetics geogrids composites tested under uniaxial tensile loading.	Displacement and strain distribution. Maximum principal strain	**Not reported, Not reported, Not reported,**
(Fallah Pour et al., 2020)	Ten FRP-confined concrete composite specimens tested under uniaxial compression load.	Axial, lateral, and Von Mises strains.	**2.8-MP, Not reported, VIC-3D** (Correlated Solutions, n.d.-b)
(Janeliukstis & Chen, 2021)	Review static and dynamic tests of large-scale composite structure under various loadings such as buckling, crash, rotating, impact, and fatigue loads.	Full-field deformations. Displacement field. dynamic measurements.	**3.2-MP, 4-MP, 5-MP, 12-MP, 3.84 px/mm, GOM 2D & 3D** (Metrology, 2019)
(Spencer et al., 2021)	Big Area Additive Manufacturing (BAAM) system while printing a full-size wall that has a building envelope of 6.1 x 2.4 x 1.8 (long x wide x tall).	Thermal residual stresses monitoring.	**12.2-MP, 13.6 - 32 px/mm, VIC-2D** (Correlated Solutions, n.d.-a)
(Lim et al., 2022)	Six FRP grids specimens consisting of BFRP and CFRP composites having a 300 mm length tested under uniaxial tensile loading.	Young's Modulus. Vertical strain.	**18-MP, Not reported, Ncorr** (Blaber et al., 2015)
(Chen et al., 2023)	A steel plate with 500mm long, 90mm width, and 7.5mm thickness with an edge crack that is repaired with CFRP sheet is subjected to uniaxial tensile load.	Displacement field. Crack growth propagation trajectories.	**8-MP, Not reported, VIC-2D** (Correlated Solutions, n.d.-a)
5. Structural joints			
Author	**Specimen type and test method**	**Measured parameters**	**DIC specifications (Camera resolution, Measurement**

			resolution, DIC software)
(Sozen & Guler, 2011)	bolted steel connections specimens tested under uniaxial tensile load.	In-plane displacement distributions.	**0.78-MP, Not reported, MATLAB** (The Math Works, 2020)
(Desai, 2016)	A steel beam-to-column connection specimen act as a cantilever loaded at its free.	Minimum measurable strains at six locations at the joint.	**36.3-MP, Not reported, GOM 2D** (Metrology, 2019)
(Peng et al., 2018)	Two welded steel joints 20 mm thick and 25 x 20 section, tested under uniaxial tensile load.	The strain distribution.	**Not reported, Not reported, PMLAB DIC-3D_2014a** (PMLAB, 2014)**.**
(Biscaia et al., 2018)	Interfacial behaviour between a reinforcement material and a substrate through a series of single-lap shear tests.	Slip distribution.	**18-MP, Not reported, GOM 2D** (Metrology, 2019), **Ncorr** (Blaber et al., 2015)
(Kavdir & Aydin, 2019)	Adhesively bonded single lap joints tested under tensile and shear loads.	Shear strain distributions. Strain distributions in the adhesive layer.	**Not reported, Not reported, GOM 2D** (Metrology, 2019)
(Ziaja et al., 2020)	Pretensioned bolted beam-to-column connection anomaly detection during frame's vibrations caused by harmonic excitation	Damage and anomaly detection in connections.	**1-MP, 15 px/mm, DANTEC Istra 4D** (Nova Instruments, 2016)
(Chang & Huang, 2020)	A downscaled model of RC structure subjected to seismic vibrations.	Biaxial deformation at the beam-column region. Displacement and angle of inter-story drift.	**0.3-MP, Not reported, MATLAB** (The Math Works, 2020)
(F. Sun & Blackman, 2020)	A double cantilever beam (DCB) with aluminium alloy substrate tested with a screw-driven tensile test machine.	Crack length measurement. Crack tip separation. Beam rotation.	**18-MP, 28.5 px/mm, GOM 2D** (Metrology, 2019)

Preprints (www.preprints.org) | NOT PEER-REVIEWED | Posted: 25 September 2023 doi:10.20944/preprints202309.1590.v1

		Energy release rate.	
(Kim et al., 2021)	A single-lap hybrid bonded-bolted (HBB) joints that has a bolted hole in the centre. The samples were tested under uniaxial load.	Shear strain around the bolt. Surface failure location identification.	**1-MP, 30.7 – 31.9 px/mm, MatchID** (Colors, n.d.)
(Wani et al., 2022)	A five-story steel-frame braced structure with 6m height and 2 x 2 m plan area, subjected to bi-directional seismic excitations.	Displacement, acceleration, and velocity time history of the beam-column joint. Inter-story drift. Strain in joint and floor.	**8 high-speed cameras, 2.3-MP, 2.2 px/mm, VIC-2D & 3D** (Correlated Solutions, n.d.-a)
(Xu et al., 2022)	Bolted fibre metal laminate joints consists of three layers of T3 aluminium of 0.4 mm thickness and four layers of GFRP. The samples were tested under uniaxial loading.	Displacement distribution. Compression and tension damage dominance regions.	**2.3-MP, Not reported, VIC-3D** (Correlated Solutions, n.d.-b)
(Paliwal & Ramji, 2022)	Three test coupons each of the bonded, bolted, and hybrid joint tested under uniaxial tensile load.	Strain field of the joint. Strain field over the adhesive layer along the thickness. Failure mechanism.	**5-MP, Not reported, VIC-2D & 3D** (Correlated Solutions, n.d.-a)
(Sousa et al., 2023)	Twenty-seven dry joint (flat, single-keyed, three-keyed) specimens of prestressed segmental bridges were subjected to push-off testes.	Joints sliding. Deformation and crack analysis,	**3.6-MP, Not reported, GOM 2D** (Metrology, 2019)
6. Steel structures			
Author	**Specimen type and test method**	**Measured parameters**	**DIC specifications (Camera resolution, Measurement resolution, DIC software)**

(Peddle et al., 2011)	A W4x13 steel beam tested under three-point bending.	Beam deflection.	**2-MP, Not reported, VIC-2D** (Correlated Solutions, n.d.-a)
(Yoneyama & Ueda, 2012)	A wide flange beam made of steel, 5m long, 0.2m in width and 8mm in thickness tested under three-point bending.	The deflections of the beam.	**8-MP, Not reported, Not reported**
(M. H. Shih & Sung, 2014)	A five-story steel framed structure subjected to a series of dynamic experiments.	Dynamic analysis and damage detection	**2-MP, Not reported, Not reported**
(Dutton et al., 2014)	A hollow steel section (HSS) beam having a 1.2m length and 0.1 x 0.1 m section loaded in three-point bending.	Longitudinal strains. Beam curvature.	**18-MP, 27.8 px/mm, GeoPIV** (Stanier et al., 2016; Take, 2015; White et al., 2003)
(Ngeljaratan & Moustafa, 2017)	Free vibration and earthquake tests of steel frame having (0.5 length x 0.3 width x 1.1 height)	Displacement, velocity, and acceleration.	**high-speed 5-MP, Not reported, Not reported**
(Gorman & Thouless, 2019)	An adhesively-bonded double-cantilever beam (DCB) having a length of 152mm loaded at its free end.	Displacement and strain. displacements within a cohesive zone. Rotation and shear strain.	**Two 5-MP, Not reported, VIC-2D** (Correlated Solutions, n.d.-a)
(Tian, Zhao, et al., 2021)	A thin cantilever steel beam having 950 mm long subjected to static loads at five locations.	Scale factor. Full-field beam deflection.	**1.3-MP, Not reported, Not reported**
7. Slabs and other members			
Author	**Specimen type and test method**	**Measured parameters**	**DIC specifications (Camera resolution, Measurement resolution, DIC software)**
(Al-Mosawe et al., 2018)	Uniaxial tensile test of dog-bone specimens.	Three speckle pattern configurations were used to measure the strain.	**5-MP, Not reported, VIC-2D & 3D** (Correlated Solutions, n.d.-a)

 doi:10.20944/preprints202309.1590.v1

(Ngeljaratan & Moustafa, 2019)	Three 1/3 RC two-span bridges tested under bidirectional earthquake.	Frequency estimation. Damping ratio, and mode shapes of the bridges.	**5-MP, Not reported, GOM 2D** (Metrology, 2019)
(Tehrani et al., 2020)	Static loading of corrugated metal pipes.	Deflection and pipe profile.	**18-MP, 3 px/mm - 4 px/mm, GOM 2D** (Metrology, 2019)
(Gehri et al., 2020; Mata-Falcón et al., 2020)	Reinforced concrete RC panel subjected to diagonal tension.	Automated crack width and slip measurement.	**29-MP, 2.63 px/mm, VIC-3D** (Correlated Solutions, n.d.-b)
(Sharafisafa et al., 2020)	Bimrock disc specimens with 40 mm diameter and 15mm thickness, tested under tensile Brazilian disc test.	Crack initiation. Maximum shear strain. Overall failure pattern of three types of Bimrocks.	**NA-MP, 60-fps. Not reported, Not reported**
(Zhang et al., 2021)	Series of semi-circular bending tests of the mine tailings rock material.	Strain distribution. Mode-I fracture toughness	**Not reported, 22.7 px/mm, VIC-3D** (Correlated Solutions, n.d.-b)
(Christensen et al., 2021)	Three Overturned T-beam RC slabs under controlled laboratory conditions. Two of the concrete slabs (0.55 × 3.6 × 9.0 m) were stripped from in situ full-scale Ot-slab bridge having a 9m span and one downscaled slab.	Crack identification and assessment.	**Two cameras 20-MP, 18.7-MP, 0.69 px/mm – 1.72 px/mm, GOM 2D** (Metrology, 2019)
(Thériault et al., 2022)	Double-L shape RC specimens, shear push-off testing.	Crack kinematics was observed using the full-field strain.	**18-MP, 24-MP, 10.8 px/mm to 11.8 px/mm, GOM 2D** (Metrology, 2019)
(Luo et al., 2023)	Six ultra-high-performance fibre-reinforced and steel rebars reinforced concrete (500 mm long, 100 mm wide, and 50 mm	Full-field displacement and strain. Cracking behaviour.	**Two 9.1-MP, 13.3 px/mm, Not reported**

Preprints (www.preprints.org) | NOT PEER-REVIEWED | Posted: 25 September 2023 doi:10.20944/preprints202309.1590.v1

	thick) specimens were tested by direct tensile tests.

From the provided data in Table 2, the following are some interesting patterns, trends, and statistics that can be observed:

Camera Resolution: The camera resolution used in the studies ranges from 0.3 MP to 29 MP, with a majority of studies using cameras with resolutions between 12 MP and 18 MP. Figure 4 shows the camera resolution count of the reviewed studies.

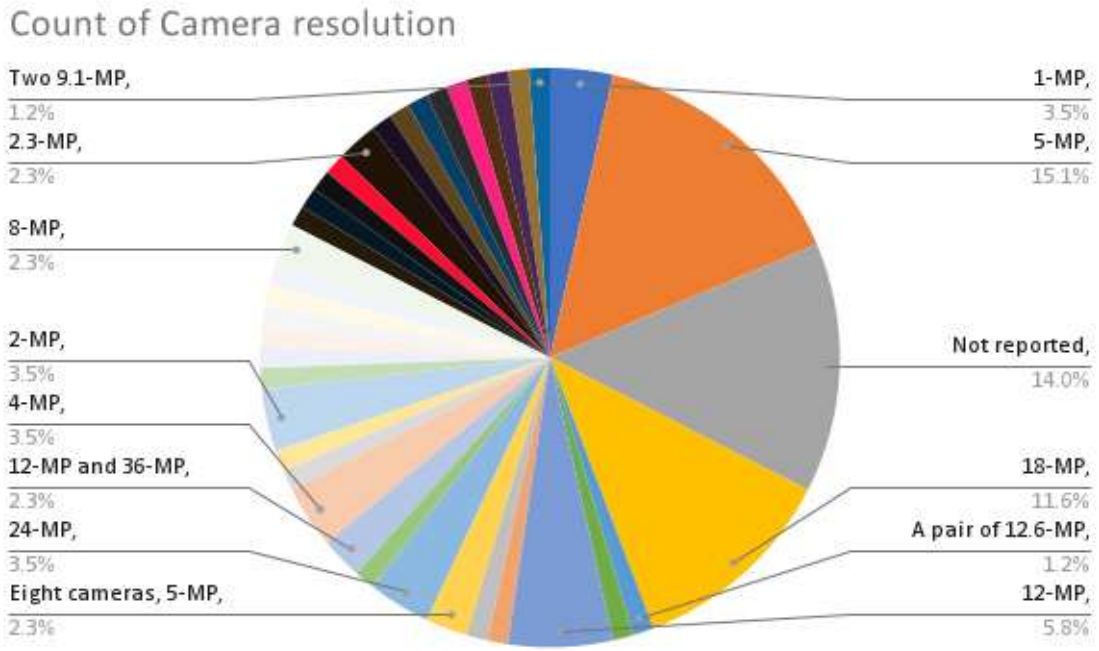

Figure 4. Count of camera resolution of the reviewed DIC studies.

Measurement Resolution: The measurement resolution varies widely across the studies, with values ranging from 0.5 px/mm to 290 px/mm. The majority of studies have measurement resolutions between 1 px/mm and 30 px/mm. Figure 5 shows the camera resolution count of the reviewed studies.

DIC Software: Several DIC software packages were used, including VIC-2D, VIC-3D, GOM 2D, GOM 3D, GeoPIV, Ncorr, DANTEC Istra 4D, and MATLAB. These software packages provide different capabilities for analysis and measurement. Figure 6 shows the DIC software count of the reviewed studies.

Preprints (www.preprints.org) | NOT PEER-REVIEWED | Posted: 25 September 2023 doi:10.20944/preprints202309.1590.v1

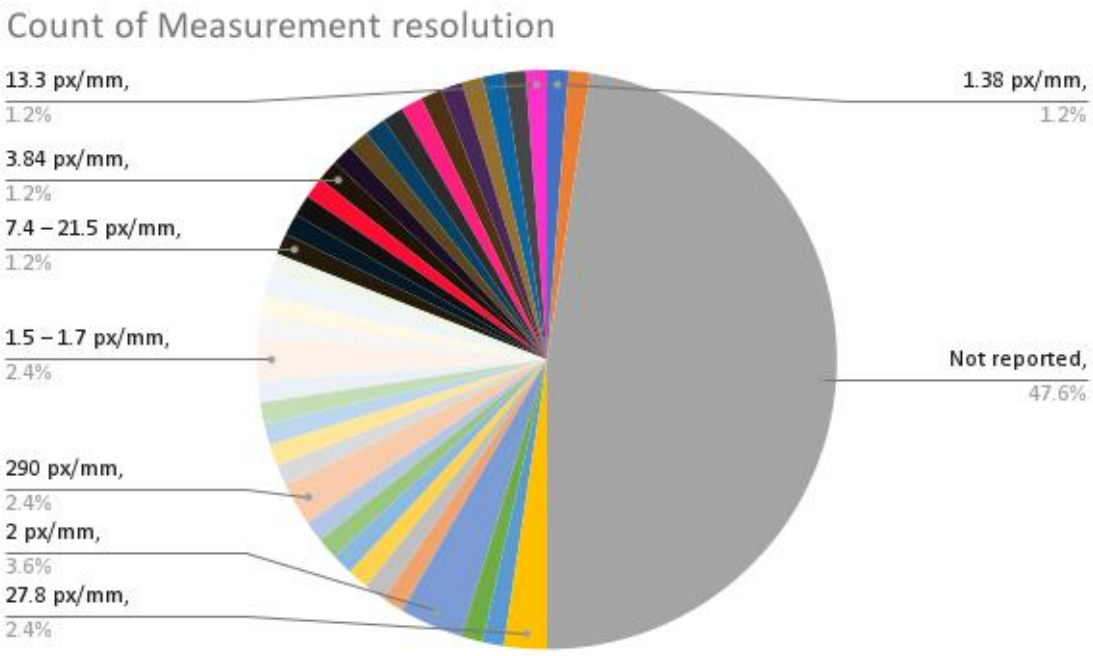

Figure 5. Count of measurement resolution of the reviewed DIC studies.

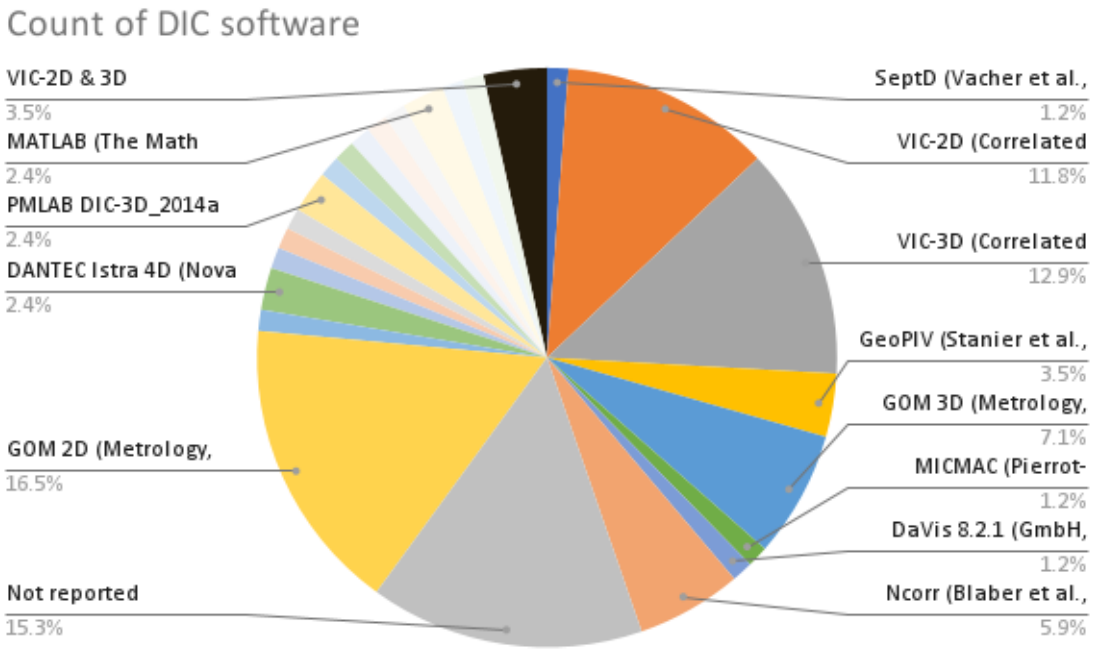

Figure 6. Count of DIC software used in the reviewed studies.

Specimen Types: The studies cover a wide range of specimen types, including RC beams, concrete prisms, masonry walls and infills, composite materials, structural joints, steel structures, and slabs. This reflects the diverse applications of DIC in structural testing. Figure 7 shows the count of the specimen types of the structural members of the reviewed studies.

Preprints (www.preprints.org) | NOT PEER-REVIEWED | Posted: 25 September 2023 doi:10.20944/preprints202309.1590.v1

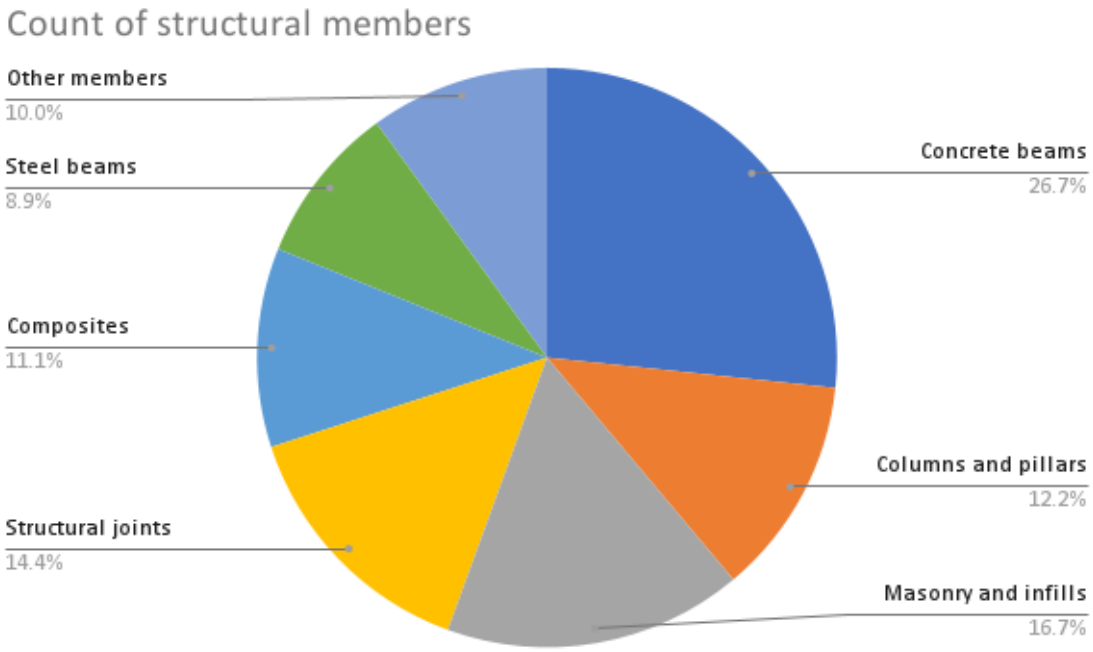

Figure 7. Count of specimen types of the structural members of the reviewed DIC works.

Measured Parameters: The studies focus on measuring various parameters such as displacement fields, strain distribution, crack width, deformation, fracture parameters, and failure mechanisms. This demonstrates the versatility of DIC in capturing different aspects of structural behaviour. Figure 8 shows the counts of the measured parameters of the reviewed studies.

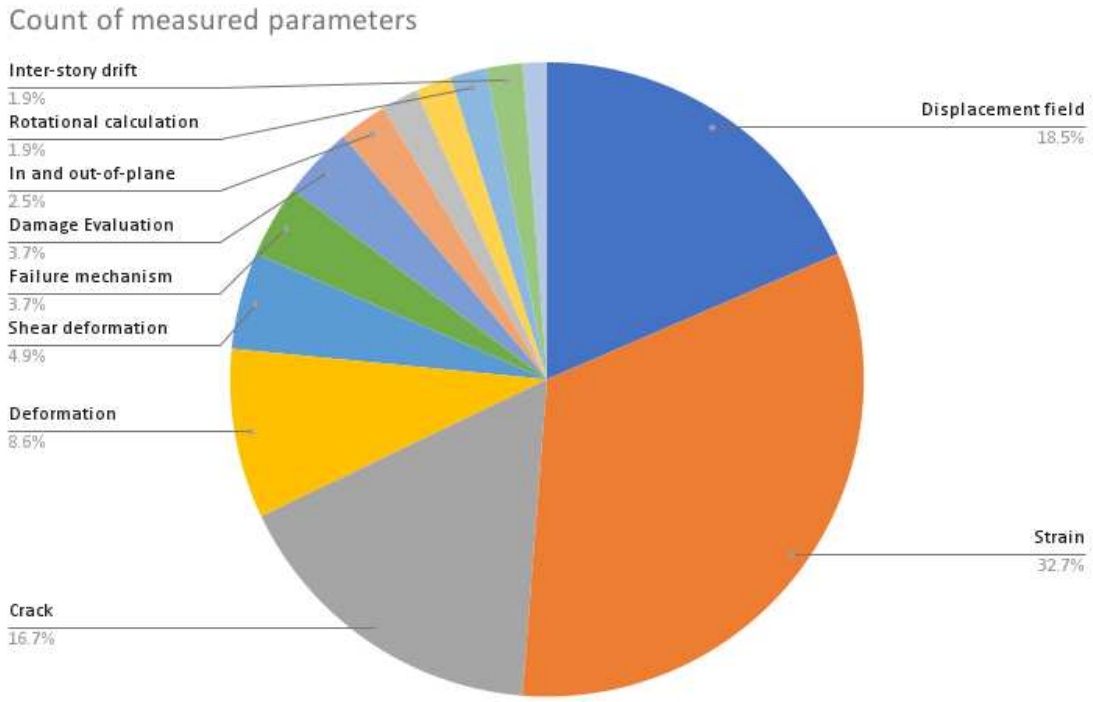

Figure 8. Counts of the measured parameters of the reviewed DIC studies.

Material Types: Different materials were tested, including concrete, steel, masonry, composites (such as FRP and GFRP), and geosynthetics. This highlights the applicability of DIC across a range of

Preprints (www.preprints.org) | NOT PEER-REVIEWED | Posted: 25 September 2023 doi:10.20944/preprints202309.1590.v1

materials used in structural engineering. Figure 9 shows the counts of the tested materials of the reviewed studies.

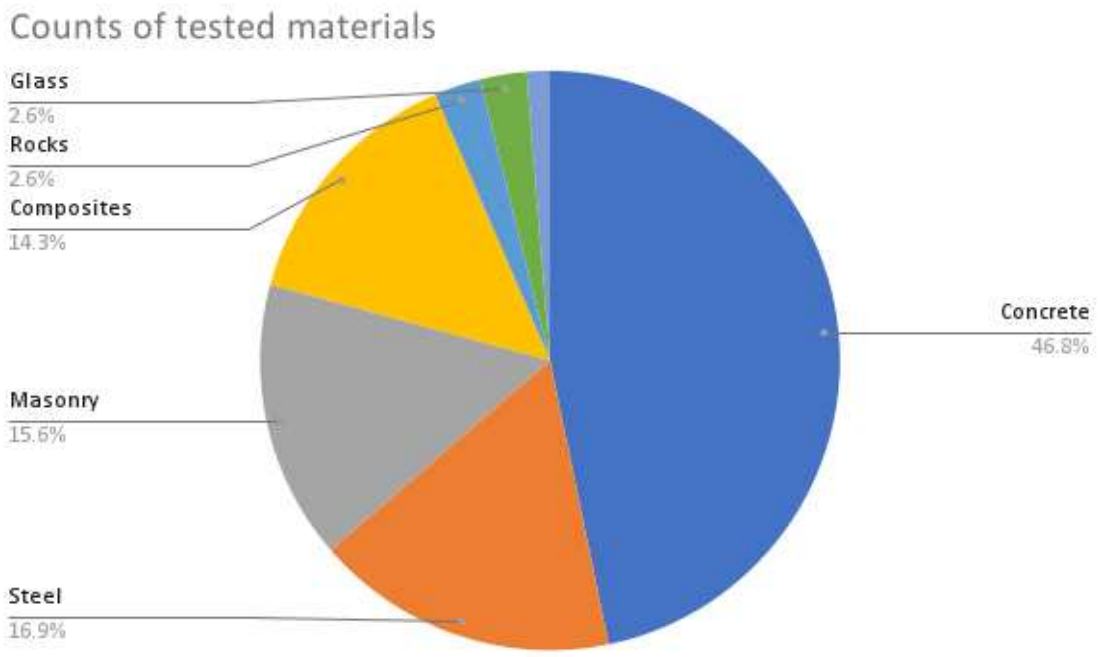

Figure 9. Counts of the tested materials of the reviewed DIC studies.

Test Methods: Various test methods were employed, such as three-point bending, four-point bending, compression tests, tensile tests, shear tests, uniaxial loading tests, and cyclic loading tests. This indicates the flexibility of DIC in accommodating different testing scenarios. Figure 10 shows the count of test types used in the reviewed studies.

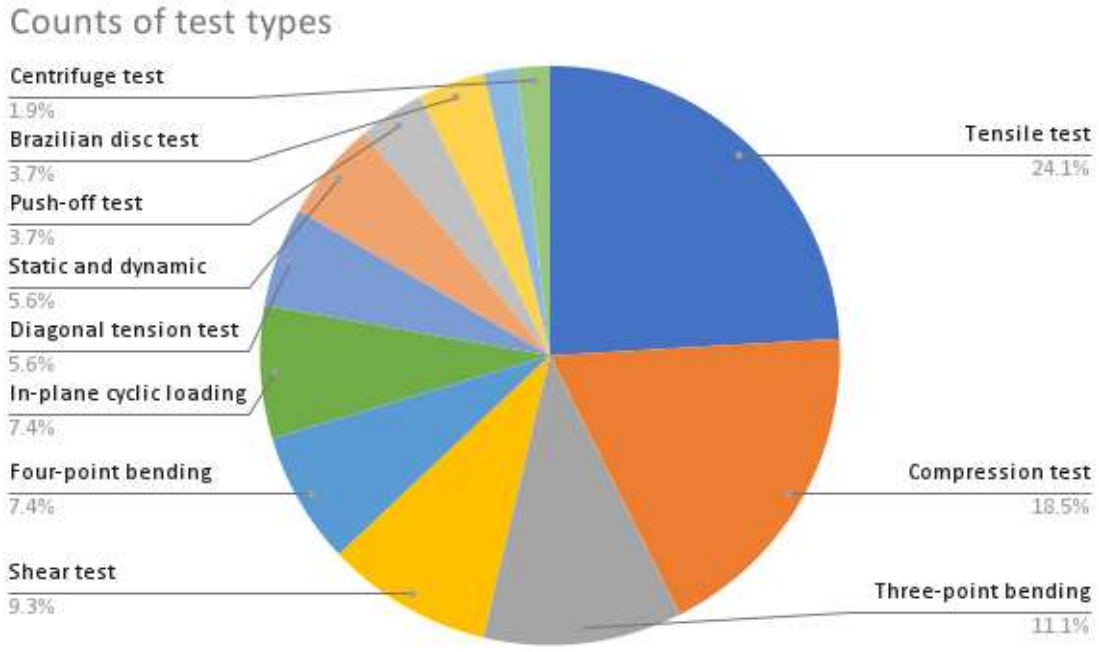

Figure 10. Counts of test types used in the reviewed DIC tests.

Application Areas: The studies cover a wide range of application areas, including monitoring of structural health, evaluation of material properties, detection of damage and cracks, assessment of performance under different loads, and analysis of failure mechanisms. Figure 11 shows the counts and percentages of application areas.

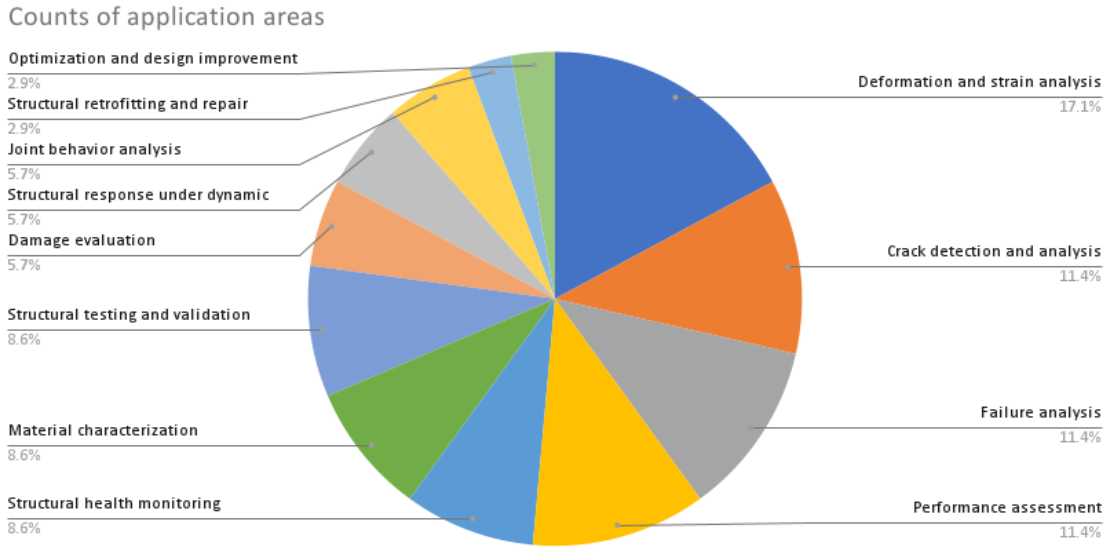

Figure 11. Count of application areas used in the reviewed DIC studies.

These patterns, trends, and statistics provide insights into the diverse use cases and capabilities of DIC in structural testing and analysis.

4. Conclusions

The use of Digital Image Correlation (DIC) in structural testing and analysis has showcased its versatility and capabilities. Studies have employed cameras with resolutions ranging from 0.3 MP to 29 MP, with a majority falling between 12 MP and 18 MP. Measurement resolutions varied widely, from 0.5 px/mm to 290 px/mm, with the majority falling between 1 px/mm and 30 px/mm. Different DIC software packages, such as VIC-2D, VIC-3D, GOM 2D, GOM 3D, GeoPIV, Ncorr, DANTEC Istra 4D, and MATLAB, were utilized for analysis and measurement. The studies covered a diverse range of specimen types, including RC beams, concrete prisms, masonry walls and infills, composite materials, structural joints, steel structures, and slabs. Measured parameters encompass displacement fields, strain distribution, crack width, deformation, fracture parameters, and failure mechanisms. DIC proved applicable to various materials used in structural engineering, including concrete, steel, masonry, composites (such as FRP and GFRP), and geosynthetics. Different test methods, such as three-point bending, four-point bending, compression tests, tensile tests, shear tests, uniaxial loading tests, and cyclic loading tests, were employed. DIC found applications in structural health monitoring, evaluating material properties, detecting damage and cracks, assessing performance under different loads, and analyzing failure mechanisms. These findings highlight the broad range of use cases and capabilities of DIC in structural testing and analysis.

References

1. Aggelis, D. G., Verbruggen, S., Tsangouri, E., Tysmans, T., & Van Hemelrijck, D. (2013). Characterization of mechanical performance of concrete beams with external reinforcement by acoustic emission and digital image correlation. *Construction and Building Materials*, *47*, 1037–1045. https://doi.org/10.1016/j.conbuildmat.2013.06.005
2. Alam, S. Y., Loukili, A., Grondin, F., & Rozière, E. (2015). Use of the digital image correlation and acoustic emission technique to study the effect of structural size on cracking of reinforced concrete. *Engineering Fracture Mechanics*, *143*, 17–31. https://doi.org/10.1016/j.engfracmech.2015.06.038

3. Alam, S. Y., Saliba, J., & Loukili, A. (2014). Fracture examination in concrete through combined digital image correlation and acoustic emission techniques. *Construction and Building Materials*, *69*, 232–242. https://doi.org/10.1016/j.conbuildmat.2014.07.044
4. Al-Kamaki, Y. S. S. (2021). Ultimate strain models derived using a Digital Image Correlation (DIC) system for preloaded RC columns subjected to heating and cooling and confined with CFRP sheets. *Journal of Building Engineering*, *41*. https://doi.org/10.1016/j.jobe.2021.102306
5. Allain, M., Ple, O., Prime, N., Roux, E., & Vacher, P. (2023). In situ DIC method to determine stress state in reinforced concrete structures. *Measurement: Journal of the International Measurement Confederation*, *210*(February 2022). https://doi.org/10.1016/j.measurement.2023.112483
6. Al-Mosawe, A., Agha, H., Al-Hadeethi, L., & Al-Mahaidi, R. (2018). Efficiency of image correlation photogrammetry technique in measuring strain. *Australian Journal of Structural Engineering*, *19*(3), 207–213. https://doi.org/10.1080/13287982.2018.1480304
7. Arora, H., Hooper, P. A., & Dear, J. P. (2011). Dynamic response of full-scale sandwich composite structures subject to air-blast loading. *Composites Part A: Applied Science and Manufacturing*, *42*(11), 1651–1662. https://doi.org/10.1016/j.compositesa.2011.07.018
8. Aryanto, A., Revolis, M., Oribe, Y., & Yo, H. (2023). Application of Digital Image Correlation Method in Rc and Frc Beams Under Bending Test. *International Journal of GEOMATE*, *24*(101), 118–125. https://doi.org/10.21660/2023.101.g12275
9. Bado, M. F., Kaklauskas, G., & Casas, J. R. (2019). Performance of Distributed Optical Fiber Sensors (DOFS) and Digital Image Correlation (DIC) in the monitoring of RC structures. *IOP Conference Series: Materials Science and Engineering*, *615*(1). https://doi.org/10.1088/1757-899X/615/1/012101
10. Beberniss, T. J., & Ehrhardt, D. A. (2017). High-speed 3D digital image correlation vibration measurement: Recent advancements and noted limitations. *Mechanical Systems and Signal Processing*, *86*, 35–48. https://doi.org/10.1016/j.ymssp.2016.04.014
11. Becks, H., Baktheer, A., Marx, S., Classen, M., Hegger, J., & Chudoba, R. (2023). Monitoring concept for the propagation of compressive fatigue in externally prestressed concrete beams using digital image correlation and fiber optic sensors. *Fatigue and Fracture of Engineering Materials and Structures*, *46*(2), 514–526. https://doi.org/10.1111/ffe.13881
12. Belloni, V., Ravanelli, R., Nascetti, A., Rita, M. Di, Mattei, D., & Crespi, M. (2019). Py2dic: A new free and open source software for displacement and strain measurements in the field of experimental mechanics. *Sensors (Switzerland)*, *19*(18). https://doi.org/10.3390/s19183832
13. Besnard, G., Hild, F., & Roux, S. (2006). "Finite-element" displacement fields analysis from digital images: Application to Portevin-Le Châtelier bands. *Experimental Mechanics*, *46*(6), 789–803. https://doi.org/10.1007/s11340-006-9824-8
14. Biscaia, H. C., Franco, N., & Chastre, C. (2018). Development of a simple bond-slip model for joints monitored with the DIC technique. *Archives of Civil and Mechanical Engineering*, *18*(4), 1535–1546. https://doi.org/10.1016/j.acme.2018.06.009
15. Blaber, J., Adair, B., & Antoniou, A. (2015). Ncorr: Open-Source 2D Digital Image Correlation Matlab Software. *Experimental Mechanics*, *55*(6), 1105–1122. https://doi.org/10.1007/s11340-015-0009-1
16. Bolhassani, M., Rajaram, S., Hamid, A. A., Kontsos, A., & Bartoli, I. (2016). Damage detection of concrete masonry structures by enhancing deformation measurement using DIC. *Nondestructive Characterization and Monitoring of Advanced Materials, Aerospace, and Civil Infrastructure 2016*, *9804*(215), 980411. https://doi.org/10.1117/12.2218368
17. Boukhtache, S., Abdelouahab, K., Berry, F., Blaysat, B., Grédiac, M., & Sur, F. (2020). When Deep Learning Meets Digital Image Correlation. *Optics and Lasers in Engineering*, *136*(July), 106308. https://doi.org/10.1016/j.optlaseng.2020.106308
18. Chang, C. Y., & Huang, C. W. (2020). Non-contact measurement of inter-story drift in three-layer RC structure under seismic vibration using digital image correlation. *Mechanical Systems and Signal Processing*, *136*, 106500. https://doi.org/10.1016/j.ymssp.2019.106500
19. Chen, T., Ye, M., Yao, C., & Xiao, Z. (2023). Fatigue behavior and digital image correlation monitoring of steel plates with mixed-mode edge cracks repaired with CFRP materials. *Composite Structures*, *304*(P1), 116408. https://doi.org/10.1016/j.compstruct.2022.116408
20. Christensen, C. O., Schmidt, J. W., Halding, P. S., Kapoor, M., & Goltermann, P. (2021). Digital image correlation for evaluation of cracks in reinforced concrete bridge slabs. *Infrastructures*, *6*(7). https://doi.org/10.3390/infrastructures6070099
21. Chu, T., Peters, W. H., Ranson, W. F., & Sutton, M. A. (1982). Application of Digital Correlation Methods To Rigid Body Mechanics. *Proceedings of the Society for Experimental Stress Analysis*, 73–76. https://doi.org/10.1117/12.7973231
22. Colors, M. beyond. (n.d.). *MatchID 2D*. www.matchidmbc.com
23. Correlated Solutions. (n.d.-a). *VIC-2D*. Retrieved December 23, 2022, from https://www.correlatedsolutions.com/vic-2d

24. Correlated Solutions. (n.d.-b). *VIC-3D*. Retrieved December 23, 2022, from https://www.correlatedsolutions.com/vic-3d
25. Daghash, S. M., & Ozbulut, O. E. (2017). Flexural performance evaluation of NSM basalt FRP-strengthened concrete beams using digital image correlation system. *Composite Structures*, *176*, 748–756. https://doi.org/10.1016/j.compstruct.2017.06.021
26. Dai, Y., & Li, H. (2022). Multi-Camera Digital Image Correlation in Deformation Measurement of Civil Components with Large Slenderness Ratio and Large Curvature. *Materials*, *15*(18), 6281. https://doi.org/10.3390/ma15186281
27. Dai, Y. T., Wang, H. T., Ge, T. Y., Wu, G., Wan, J. X., Cao, S. Y., Yang, F. J., & He, X. Y. (2017). Stereo-digital image correlation in the behavior investigation of CFRP-steel composite members. *Steel and Composite Structures*, *23*(6), 727–736. https://doi.org/10.12989/scs.2017.23.6.727
28. del Rey Castillo, E., Allen, T., Henry, R., Griffith, M., & Ingham, J. (2019). Digital image correlation (DIC) for measurement of strains and displacements in coarse, low volume-fraction FRP composites used in civil infrastructure. *Composite Structures*, *212*, 43–57. https://doi.org/10.1016/j.compstruct.2019.01.024
29. Demchyna, B., Surmai, M., & Tkach, R. (2019). The experimental study of glass multilayer columns using digital image correlation. *Archives of Materials Science and Engineering*, *96*(1), 32–41. https://doi.org/10.5604/01.3001.0013.1990
30. Demchyna, B., Surmai, M., Tkach, R., Hula, V., & Kozak, R. (2020). an Analysis of Using the Method of Two-Dimensional Digital Image Correlation in Glass Column Research. *Eastern-European Journal of Enterprise Technologies*, *4*(12–106), 52–59. https://doi.org/10.15587/1729-4061.2020.209761
31. Desai, N. (2016). Small-strain measurement in bridge connections using the digital image correlation (DIC) technique. *Health Monitoring of Structural and Biological Systems 2016*, *9805*(Dic), 980530. https://doi.org/10.1117/12.2234454
32. Destrebecq, J. F., Toussaint, E., & Ferrier, E. (2011). Analysis of Cracks and Deformations in a Full Scale Reinforced Concrete Beam Using a Digital Image Correlation Technique. *Experimental Mechanics*, *51*(6), 879–890. https://doi.org/10.1007/s11340-010-9384-9
33. Domaneschi, M., Cimellaro, G. P., de Iuliis, M., & Marano, G. C. (2021). Laboratory investigation of digital image correlation techniques for structural assessment. *Bridge Maintenance, Safety, Management, Life-Cycle Sustainability and Innovations - Proceedings of the 10th International Conference on Bridge Maintenance, Safety and Management, IABMAS 2020*, 3260–3266. https://doi.org/10.1201/9780429279119-442
34. Dutton, M., Take, W. A., & Hoult, N. A. (2014). Curvature Monitoring of Beams Using Digital Image Correlation. *Journal of Bridge Engineering*, *19*(3). https://doi.org/10.1061/(asce)be.1943-5592.0000538
35. Enfedaque, A., Alberti, M. G., Gálvez, J. C., del Río, M. A., & Xiaobo, T. (2022). Use of digital image correlation to connect fracture curves and sectional analysis for structural design of polyolefin fibre reinforced concrete elements. *Construction and Building Materials*, *328*. https://doi.org/10.1016/j.conbuildmat.2022.127039
36. Enfedaque, A., Gálvez, J. C., & Suárez, F. (2015). Analysis of fracture tests of glass fibre reinforced cement (GRC) using digital image correlation. *Construction and Building Materials*, *75*, 472–487. https://doi.org/10.1016/j.conbuildmat.2014.11.031
37. Fallah Pour, A., Nguyen, G. D., Vincent, T., & Ozbakkaloglu, T. (2020). Investigation of the compressive behavior and failure modes of unconfined and FRP-confined concrete using digital image correlation. *Composite Structures*, *252*(April), 112642. https://doi.org/10.1016/j.compstruct.2020.112642
38. Felipe-Sesé, L., Molina-Viedma, Á., López-Alba, E., & Díaz, F. (2018). Dynamic Displacements Measurement Employing Fringe Projection and Digital Image Correlation. *Proceedings*, *2*(8), 458. https://doi.org/10.3390/icem18-05366
39. Ferreira, M. D. C., Venturini, W. S., & Hild, F. (2011). On the analysis of notched concrete beams: From measurement with digital image correlation to identification with boundary element method of a cohesive model. *Engineering Fracture Mechanics*, *78*(1), 71–84. https://doi.org/10.1016/j.engfracmech.2010.10.008
40. Furtado, A., Ramos, T., Rodrigues, H., Arêde, A., Varum, H., & Tavares, P. (2015). In-plane Response of Masonry Infill Walls: Experimental Study using Digital Image Correlation. *Procedia Engineering*, *114*(December), 870–876. https://doi.org/10.1016/j.proeng.2015.08.042
41. Gali, S., & Subramaniam, K. V. L. (2017). Shear behavior of steel fiber reinforced concrete using full-field displacements from digital image correlation. *MATEC Web of Conferences*, *120*, 1–13. https://doi.org/10.1051/matecconf/201712004003
42. Gehri, N., Mata-Falcón, J., & Kaufmann, W. (2020). Automated crack detection and measurement based on digital image correlation. *Construction and Building Materials*, *256*, 119383. https://doi.org/10.1016/j.conbuildmat.2020.119383
43. Gencturk, B., Hossain, K., Kapadia, A., Labib, E., & Mo, Y. L. (2014). Use of digital image correlation technique in full-scale testing of prestressed concrete structures. *Measurement: Journal of the International Measurement Confederation*, *47*(1), 505–515. https://doi.org/10.1016/j.measurement.2013.09.018

44. Ghahremannejad, M., Mahdavi, M., Saleh, A. E., Abhaee, S., & Abolmaali, A. (2018). Experimental investigation and identification of single and multiple cracks in synthetic fiber concrete beams. *Case Studies in Construction Materials*, *9*, e00182. https://doi.org/10.1016/j.cscm.2018.e00182
45. Ghiassi, B., Xavier, J., Oliveira, D. v., & Lourenço, P. B. (2013). Application of digital image correlation in investigating the bond between FRP and masonry. *Composite Structures*, *106*, 340–349. https://doi.org/10.1016/j.compstruct.2013.06.024
46. Gholizadeh, S. (2016). A review of non-destructive testing methods of composite materials. *Procedia Structural Integrity*, *1*, 50–57. https://doi.org/10.1016/j.prostr.2016.02.008
47. Ghorbani, R., Matta, F., & Sutton, M. A. (2015). Full-Field Deformation Measurement and Crack Mapping on Confined Masonry Walls Using Digital Image Correlation. *Experimental Mechanics*, *55*(1), 227–243. https://doi.org/10.1007/s11340-014-9906-y
48. GmbH, L. (2009). *DaVis 8.2.1*.
49. Gorman, J. M., & Thouless, M. D. (2019). The use of digital-image correlation to investigate the cohesive zone in a double-cantilever beam, with comparisons to numerical and analytical models. *Journal of the Mechanics and Physics of Solids*, *123*, 315–331. https://doi.org/10.1016/j.jmps.2018.08.013
50. Górszczyk, J., & Malicki, K. (2019). Digital image correlation method in monitoring deformation during geogrid testing. *Fibres and Textiles in Eastern Europe*, *27*(2), 84–90. https://doi.org/10.5604/01.3001.0012.9992
51. Guerrero, N., Martínez, M., Picón, R., Marante, M. E., Hild, F., Roux, S., & Flórez-López, J. (2014). Experimental analysis of masonry infilled frames using digital image correlation. *Materials and Structures/Materiaux et Constructions*, *47*(5), 873–884. https://doi.org/10.1617/s11527-013-0099-0
52. Hamrat, M., Boulekbache, B., Chemrouk, M., & Amziane, S. (2016). Flexural cracking behavior of normal strength, high strength and high strength fiber concrete beams, using Digital Image Correlation technique. *Construction and Building Materials*, *106*, 678–692. https://doi.org/10.1016/j.conbuildmat.2015.12.166
53. Helfrick, M. N., Niezrecki, C., Avitabile, P., & Schmidt, T. (2011). 3D digital image correlation methods for full-field vibration measurement. *Mechanical Systems and Signal Processing*, *25*(3), 917–927. https://doi.org/10.1016/j.ymssp.2010.08.013
54. Herbert, D. M., Gardner, D. R., Harbottle, M., Thomas, J., & Hughes, T. G. (2011). The development of a new method for testing the lateral load capacity of small-scale masonry walls using a centrifuge and digital image correlation. *Construction and Building Materials*, *25*(12), 4465–4476. https://doi.org/10.1016/j.conbuildmat.2011.02.002
55. Hossain, M. A., Totoev, Y. Z., & Masia, M. J. (2021). Application of Digital Image Correlation (DIC) Technique for Semi Interlocking Masonry (SIM) Panels under Large Cyclic In-Plane Shear Displacement. *Experimental Techniques*, *45*(4), 509–530. https://doi.org/10.1007/s40799-020-00423-3
56. Hou, S., Fan, J., Wu, G., Wang, H., & Han, Y. (2021). Laboratory investigation of early damage detection for an old-aged reinforced concrete beam using acoustic emission and digital image correlation. *Journal of Advanced Concrete Technology*, *19*(6), 700–713. https://doi.org/10.3151/jact.19.700
57. Hoult, N. A., Dutton, M., Hoag, A., & Take, W. A. (2016). Measuring crack movement in reinforced concrete using digital image correlation: Overview and application to shear slip measurements. *Proceedings of the IEEE*, *104*(8), 1561–1574. https://doi.org/10.1109/JPROC.2016.2535157
58. Howlader, M. K., Masia, M. J., & Griffith, M. C. (2021). Digital image correlation for the analysis of in-plane tested unreinforced masonry walls. *Structures*, *29*, 427–445. https://doi.org/10.1016/j.istruc.2020.11.051
59. Janeliukstis, R., & Chen, X. (2021). Review of digital image correlation application to large-scale composite structure testing. *Composite Structures*, *271*(October 2020), 114143. https://doi.org/10.1016/j.compstruct.2021.114143
60. Kalaitzakis, M., Kattil, S. R., Vitzilaios, N., Rizos, D., & Sutton, M. (2019). Dynamic structural health monitoring using a DIC-enabled drone. *2019 International Conference on Unmanned Aircraft Systems, ICUAS 2019*, 321–327. https://doi.org/10.1109/ICUAS.2019.8798270
61. Kavdir, E. Ç., & Aydin, M. D. (2019). The investigation of mechanical properties of a structural adhesive via digital image correlation (DIC) technic. *Composites Part B: Engineering*, *173*. https://doi.org/10.1016/j.compositesb.2019.106995
62. Kearsley, E., & Jacobsz, S. W. (2018). Condition assessment of reinforced concrete beams-Comparing digital image analysis with optic fibre Bragg gratings. *MATEC Web of Conferences*, *199*. https://doi.org/10.1051/matecconf/201819906011
63. Kim, J. H., Lopez-Cruz, P., Heidari-Rarani, M., Lessard, L., & Laliberté, J. (2021). An experimental study on the mechanical behaviour of bonded and hybrid bonded-bolted composite joints using digital image correlation (DIC) technique. *Composite Structures*, *276*. https://doi.org/10.1016/J.COMPSTRUCT.2021.114544
64. Kumar, S. L., Aravind, H. B., & Hossiney, N. (2019). Digital image correlation (DIC) for measuring strain in brick masonry specimen using Ncorr open source 2D MATLAB program. *Results in Engineering*, *4*(August), 100061. https://doi.org/10.1016/j.rineng.2019.100061

65. Li, H., Dai, Y., Qiu, H., & He, X. (2022). Application of Multi-camera Digital Image Correlation in the Stability Study of the Long Timber Column with the Circular Cross-section under Axial Compression. *BioResources*, *17*(1), 1717–1728. https://doi.org/10.15376/biores.17.1.1717-1728
66. Lim, C., Jeong, Y., Limkantanyu, S., & Kwon, M. (2022). Strain Measuring of Composite Grid Using Digital Image Correlation. *Advances in Materials Science and Engineering*, *2022*. https://doi.org/10.1155/2022/6041887
67. Luo, X., Zhang, S., Li, A., Yang, X., & Liang, Z. (2023). Steel rebar effect on tensile and cracking behavior of UHPFRC based on direct tensile tests and digital image correlation. *Cement and Concrete Composites*, *137*(October 2022), 104940. https://doi.org/10.1016/j.cemconcomp.2023.104940
68. Mata-Falcón, J., Haefliger, S., Lee, M., Galkovski, T., & Gehri, N. (2020). Combined application of distributed fibre optical and digital image correlation measurements to structural concrete experiments. *Engineering Structures*, *225*(December 2019). https://doi.org/10.1016/j.engstruct.2020.111309
69. Mehdi Mirzazadeh, M., & Green, M. F. (2018). Fiber Optic Sensors and Digital Image Correlation for Measuring Deformations in Reinforced Concrete Beams. *Journal of Bridge Engineering*, *23*(3). https://doi.org/10.1061/(asce)be.1943-5592.0001189
70. Metrology, P. I. 3D. (2019). *GOM Correlate*. https://www.gom.com/3d-software/gom-correlate.html
71. Miikki, K., Karakoç, A., Rafiee, M., Lee, D. W., Vapaavuori, J., Tersteegen, J., Lemetti, L., & Paltakari, J. (2021). An open-source camera system for experimental measurements. *SoftwareX*, *14*, 100688. https://doi.org/10.1016/j.softx.2021.100688
72. Mojsilović, N., & Salmanpour, A. H. (2016). Masonry walls subjected to in-plane cyclic loading: Application of digital image correlation for deformation field measurement. *International Journal of Masonry Research and Innovation*, *1*(2), 165–187. https://doi.org/10.1504/IJMRI.2016.077473
73. Mousa, M. A., & Yussof, M. M. (2021). A simple two-dimensional digital image correlation model for out of plane displacement using smartphone camera. *Journal of Engineering Science and Technology*, *16*, 10–17.
74. Mousa, M. A., Yussof, M. M., Assi, L. N., & Ghahari, S. A. (2022). A Pre-Process Enhanced Digital Image Correlation Approach for Smart Structure Monitoring. *Infrastructures*, *7*(10). https://doi.org/10.3390/infrastructures7100141
75. Mousa, M. A., Yussof, M. M., Ruii, C. Z., Nazri, F. M., & Kamarudin, M. K. (2021). Prediction of crack path on concrete prism based on strain field using image analysis technique. *Malaysian Construction Research Journal*, *14*(3 Special issue), 85–97.
76. Murali Krishna, B., Tezeswi, T. P., Rathish Kumar, P., Gopikrishna, K., Sivakumar, M. V. N., & Shashi, M. (2019). QR code as speckle pattern for reinforced concrete beams using digital image correlation. *Structural Monitoring and Maintenance*, *6*(1), 67–84. https://doi.org/10.12989/smm.2019.6.1.067
77. Ngeljaratan, L., & Moustafa, M. A. (2017). Digital image correlation for dynamic shake table test measurements. *International Conference on Advances in Experimental Structural Engineering*, *2017-Septe*(July), 741–752. https://doi.org/10.7414/7aese.T6.115
78. Ngeljaratan, L., & Moustafa, M. A. (2019). System identification of large-scale bridges using target-tracking digital image correlation. *Frontiers in Built Environment*, *5*(June). https://doi.org/10.3389/fbuil.2019.00085
79. Nghiem, H. L., Al Heib, M., & Emeriault, F. (2015). Method based on digital image correlation for damage assessment in masonry structures. *Engineering Structures*, *86*, 1–15. https://doi.org/10.1016/j.engstruct.2014.12.021
80. Nova Instruments. (2016). *Istra4D software manual Q-400 system, dantec dynamics,* (version 4.4.5). Nova Instruments Company.
81. Olufsen, S. N., Andersen, M. E., & Fagerholt, E. (2020). µDIC: An open-source toolkit for digital image correlation. *SoftwareX*, *11*. https://doi.org/10.1016/j.softx.2019.100391
82. Omondi, B., Aggelis, D. G., Sol, H., & Sitters, C. (2016). Improved crack monitoring in structural concrete by combined acoustic emission and digital image correlation techniques. *Structural Health Monitoring*, *15*(3), 359–378. https://doi.org/10.1177/1475921716636806
83. Padmappriya, S., & Sumalatha, K. (2018). Digital Image Processing Real Time Applications. *International Journal of Engineering Science Invention*, 46–51.
84. Paliwal, I., & Ramji, M. (2022). A detailed study on the damage evolution and failure assessment of single-lap hybrid joints in CFRP laminates under tensile loading. *Composite Structures*, *299*(July), 116021. https://doi.org/10.1016/j.compstruct.2022.116021
85. Pan, B., & Tian, L. (2016). Advanced video extensometer for non-contact, real-time, high-accuracy strain measurement. *Optics Express*. https://doi.org/10.1364/oe.24.019082
86. Pan, B., Tian, L., & Song, X. (2016). Real-time, non-contact and targetless measurement of vertical deflection of bridges using off-axis digital image correlation. *NDT and E International*, *79*, 73–80. https://doi.org/10.1016/j.ndteint.2015.12.006
87. Pan, B., Yu, L., & Wu, D. (2014). High-accuracy 2D digital image correlation measurements using low-cost imaging lenses: Implementation of a generalized compensation method. *Measurement Science and Technology*, *25*(2). https://doi.org/10.1088/0957-0233/25/2/025001

88. Peddle, J., Goudreau, A., Carlson, E., & Santini-Bell, E. (2011). Bridge displacement measurement through digital image correlation. *Bridge Structures*, *7*(4), 165–173. https://doi.org/10.3233/BRS-2011-031
89. Peng, Y., Wu, C., Gan, J., & Dong, J. (2018). Determination of the local constitutive properties of the welded steel joints using digital image correlation method. *Construction and Building Materials*, *171*, 485–492. https://doi.org/10.1016/j.conbuildmat.2018.03.182
90. Peters, W. H., & Ranson, W. F. (1982). Digital imaging techniques in experimental stress analysis. *Optical Engineering*, *21*(3), 427–431.
91. Pierrot-Deseilligny, M., & Paparoditis, N. (2006). A multiresolution and optimization-based image matching approach: An application to surface reconstruction from SPOT5-HRS stereo imagery. *International Archives of …*, *XXXVI*, 1–5. http://www.micmac.ign.fr/svn/micmac/tags/1.0.0/Documentation/DocMicMac/ankara2006-pierrot.pdf
92. Pisonero, J., Lopez-Rebollo, J., Garcia-Martin, R., Rodriguez-Martin, M., Sanchez-Aparicio, L. J., Munoz-Nieto, A., & Gonzalez-Aguilera, Di. (2017). A Comparative Study of 2D and 3D Digital Image Correlation Approaches for the Characterization and Numerical Analysis of Composite Materials. *IEEE Access*, *9*(Dic), 160675–160687. https://doi.org/10.1109/ACCESS.2021.3132393
93. PMLAB. (2014). *Digital Image Correlation Software PMLAB DIC-3D_2014a*. Nanjing PMLAB*Sensor Tech. Co., Ltd. http://www.pmlab.com.cn
94. Pohoryles, D. A., Melo, J., Rossetto, T., Fabian, M., McCague, C., Stavrianaki, K., Lishman, B., & Sargeant, B. (2017). Use of DIC and AE for Monitoring Effective Strain and Debonding in FRP and FRCM-Retrofitted RC Beams. *Journal of Composites for Construction*, *21*(1), 1–11. https://doi.org/10.1061/(asce)cc.1943-5614.0000715
95. Ramos, T., Furtado, A., Eslami, S., Alves, S., Rodrigues, H., Arêde, A., Tavares, P. J., & Moreira, P. M. G. P. (2015). 2D and 3D Digital Image Correlation in Civil Engineering - Measurements in a Masonry Wall. *Procedia Engineering*, *114*(December), 215–222. https://doi.org/10.1016/j.proeng.2015.08.061
96. Rouchier, S., Foray, G., Godin, N., Woloszyn, M., & Roux, J. J. (2013). Damage monitoring in fibre reinforced mortar by combined digital image correlation and acoustic emission. *Construction and Building Materials*, *38*, 371–380. https://doi.org/10.1016/j.conbuildmat.2012.07.106
97. Ruocci, G., Rospars, C., Moreau, G., Bisch, P., Erlicher, S., Delaplace, A., & Henault, J. M. (2016). Digital Image Correlation and Noise-filtering Approach for the Cracking Assessment of Massive Reinforced Concrete Structures. *Strain*, *52*(6), 503–521. https://doi.org/10.1111/str.12192
98. Salmanpour, A. H., & Mojsilović, N. (2013). Application of Digital Image Correlation for strain measurements of large masonry walls. *In: Proceedings of the 5th Asia Pacific Congress on Computational Mechanics*, *December 2013*, Paper no. 1128. http://www.sci-en-tech.com/apcom2013/APCOM2013-Proceedings/PDF_FullPaper/1128.pdf
99. Sharafisafa, M., Aliabadian, Z., & Shen, L. (2020). Crack initiation and failure of block-in-matrix rocks under Brazilian test using digital image correlation. *Theoretical and Applied Fracture Mechanics*, *109*(July). https://doi.org/10.1016/j.tafmec.2020.102743
100. Shih, M. H., & Sung, W. P. (2014). Developing dynamic digital image correlation technique to monitor structural damage of old buildings under external excitation. *Shock and Vibration*, *2014*. https://doi.org/10.1155/2014/954840
101. Shih, M. H., Sung, W. P., & Tsai, F. J. (2011). Analysis accuracy of digital image correlation technique to monitor natural frequency response of building under dynamic excitation. *Applied Mechanics and Materials*, *71–78*, 3904–3908. https://doi.org/10.4028/www.scientific.net/AMM.71-78.3904
102. Shih, M., & Sung, W. (2014). Developing Dynamic Digital Image Correlation Technique to Monitor Structural Damage of Old Buildings under External Excitation. *Shock and Vibration*, *2014*.
103. Shuai, J., Zhao, J., & Lei, L. (2022). Simple crack tip and stress intensity factor determination method for model I crack using digital image correlation. *Theoretical and Applied Fracture Mechanics*, *122*(September), 103621. https://doi.org/10.1016/j.tafmec.2022.103621
104. Słoński, M., & Tekieli, M. (2020). 2D digital image correlation and region-based convolutional neural network in monitoring and evaluation of surface cracks in concrete structural elements. *Materials*, *13*(16). https://doi.org/10.3390/MA13163527
105. Smith, B. J., Kurama, Y. C., & McGinnis, M. J. (2011). Design and Measured Behavior of a Hybrid Precast Concrete Wall Specimen for Seismic Regions. *Journal of Structural Engineering*, *137*(10), 1052–1062. https://doi.org/10.1061/(asce)st.1943-541x.0000327
106. Solav, D., Moerman, K. M., Jaeger, A. M., Genovese, K., & Herr, H. M. (2018). MultiDIC: An open-source toolbox for multi-view 3D digital image correlation. *IEEE Access*, *6*, 30520–30535. https://doi.org/10.1109/ACCESS.2018.2843725
107. Solutions, C. (2017). *Vic-2D Software*.
108. Sousa, J. B., Garcia, S. L. G., & Pierott, R. M. R. (2023). Shear Behavior of Recycled Coarse Aggregates Concrete Dry Joints Keys Using Digital Image Correlation Technique. *Infrastructures*, *8*(3), 1–24. https://doi.org/10.3390/infrastructures8030060

109. Sozen, S., & Guler, M. (2011). Determination of displacement distributions in bolted steel tension elements using digital image techniques. *Optics and Lasers in Engineering*, *49*(12), 1428–1435. https://doi.org/10.1016/j.optlaseng.2011.07.002
110. Spencer, R., Hassen, A. A., Baba, J., Lindahl, J., Love, L., Kunc, V., Babu, S., & Vaidya, U. (2021). An innovative digital image correlation technique for in-situ process monitoring of composite structures in large scale additive manufacturing. *Composite Structures*, *276*(March), 114545. https://doi.org/10.1016/j.compstruct.2021.114545
111. Stanier, S. A., Blaber, J., Take, W. A., & White, D. J. (2016). Improved image-based deformation measurement for geotechnical applications. *Canadian Geotechnical Journal*, *53*(5), 727–739. https://doi.org/10.1139/cgj-2015-0253
112. Sun, F., & Blackman, B. R. K. (2020). A DIC method to determine the Mode I energy release rate G , the J - integral and the traction-separation law simultaneously for adhesive joints. *Engineering Fracture Mechanics*, *December 2019*, 107097. https://doi.org/10.1016/j.engfracmech.2020.107097
113. Sun, Z., Zheng, Y., Sun, Y., Shao, X., & Wu, G. (2023). Deformation ability of precast concrete columns reinforced with steel-FRP composite bars (SFCBs) based on the DIC method. *Journal of Building Engineering*, *68*(September 2022), 106083. https://doi.org/10.1016/j.jobe.2023.106083
114. Suryanto, B., Tambusay, A., & Suprobo, P. (2017). Crack Mapping on Shear-critical Reinforced Concrete Beams using an Open Source Digital Image Correlation Software. *Civil Engineering Dimension*, *19*(2), 93–98. https://doi.org/10.9744/ced.19.2.93-98
115. Take, W. A. (2015). Thirty-Sixth Canadian Geotechnical Colloquium: Advances in visualization of geotechnical processes through digital image correlation. *Canadian Geotechnical Journal*, *52*(9), 1199–1220. https://doi.org/10.1139/cgj-2014-0080
116. Tehrani, A. D., Kouchesfehani, Z. K., & Najafi, M. (2020). Pipe Profiling Using Digital Image Correlation. *Pipelines 2020: Condition Assessment, Construction, Rehabilitation, and Trenchless Technologies - Proceedings of Sessions of the Pipelines 2020 Conference*, 36–45. https://doi.org/10.1061/9780784483206.005
117. Tekieli, M., De Santis, S., de Felice, G., Kwiecień, A., & Roscini, F. (2017). Application of Digital Image Correlation to composite reinforcements testing. *Composite Structures*, *160*, 670–688. https://doi.org/10.1016/j.compstruct.2016.10.096
118. Tekieli, M., & Słoński, M. (2013). Application of Monte Carlo Filter for Computer Vision-Based Bayesian Updating of Finite Element Model. *Mechanics and Control*, *32*(4), 171. https://doi.org/10.7494/mech.2013.32.4.171
119. The Math Works, Inc. (2020). *MATLAB* (R2020b).
120. Thériault, F., Noël, M., & Sanchez, L. (2022). Simplified approach for quantitative inspections of concrete structures using digital image correlation. *Engineering Structures*, *252*(November 2021), 1–12. https://doi.org/10.1016/j.engstruct.2021.113725
121. Tian, L., Yu, L., & Pan, B. (2018). Accuracy enhancement of a video extensometer by real-time error compensation. *Optics and Lasers in Engineering*. https://doi.org/10.1016/j.optlaseng.2018.06.010
122. Tian, L., Zhang, X., & Pan, B. (2021). Cost-Effective and Ultraportable Smartphone-Based Vision System for Structural Deflection Monitoring. *Journal of Sensors*, *2021*. https://doi.org/10.1155/2021/8843857
123. Tian, L., Zhao, J., Pan, B., & Wang, Z. (2021). Full-field bridge deflection monitoring with off-axis digital image correlation. *Sensors*, *21*(15), 4664–4672. https://doi.org/10.3390/s21155058
124. Torres, B., Varona, F. B., Baeza, F. J., Bru, D., & Ivorra, S. (2020). Study on retrofitted masonry elements under shear using digital image correlation. *Sensors (Switzerland)*, *20*(7). https://doi.org/10.3390/s20072122
125. Tsangouri, E., Aggelis, D. G., Van Tittelboom, K., De Belie, N., & Van Hemelrijck, D. (2013). Detecting the activation of a self-healing mechanism in concrete by acoustic emission and digital image correlation. *The Scientific World Journal*, *2013*. https://doi.org/10.1155/2013/424560
126. Tung, S. H., Shih, M. H., & Sung, W. P. (2008). Development of digital image correlation method to analyse crack variations of masonry wall. *Sadhana - Academy Proceedings in Engineering Sciences*, *33*(6), 767–779. https://doi.org/10.1007/s12046-008-0033-2
127. Tung, S. H., Shih, M. H., & Sung, W. P. (2014). Applying the digital-image-correlation technique to measure the deformation of an old building's column retrofitted with steel plate in an in situ pushover test. *Sadhana - Academy Proceedings in Engineering Sciences*, *39*(3), 699–711. https://doi.org/10.1007/s12046-014-0242-9
128. Vacher, P., Dumoulin, S., Morestin, F., & Mguil-Touchal, S. (1999). Bidimensional strain measurement using digital images. *Proceedings of the Institution of Mechanical Engineers, Part C: Journal of Mechanical Engineering*, *213*(8), 811–817. https://doi.org/10.1243/0954406991522428
129. Wang, N., Ri, K., Liu, H., & Zhao, X. (2018a). Structural displacement monitoring using smartphone camera and digital image correlation. *IEEE Sensors Journal*, *18*(11), 4664–4672. https://doi.org/10.1109/JSEN.2018.2828139
130. Wang, N., Ri, K., Liu, H., & Zhao, X. (2018b). Structural displacement monitoring using smartphone camera and digital image correlation. *IEEE Sensors Journal*, *18*(11), 4664–4672. https://doi.org/10.1109/JSEN.2018.2828139

131. Wani, Z. R., Tantray, M., & Noroozinejad Farsangi, E. (2022). In-Plane measurements using a novel streamed digital image correlation for shake table test of steel structures controlled with MR dampers. *Engineering Structures*, *256*(May 2021), 113998. https://doi.org/10.1016/j.engstruct.2022.113998
132. White, D. J., Take, W. A., & Bolton, M. D. (2003). Soil deformation measurement using particle image velocimetry (PIV) and photogrammetry. *Geotechnique*, *53*(7), 619–631. https://doi.org/10.1680/geot.2003.53.7.619
133. Winkler, J., Specialist, C., & Hansen, M. D. (2018). Innovative long-term monitoring of the great belt bridge expansion joint using digital image correlation. *Structural Engineering International*, *28*(3), 347–352. https://doi.org/10.1080/10168664.2018.1461539
134. Wittevrongel, L., Badaloni, M., Balcaen, R., Lava, P., & Debruyne, D. (2015). Evaluation of Methodologies for Compensation of Out of Plane Motions in a 2D Digital Image Correlation Setup. *Strain*, 357–369. https://doi.org/10.1111/str.12146
135. Xie, X., Guo, Z.-X., & Basha, S. H. (2023). Out-of-Plane behavior of clay brick masonry infills contained within RC frames using 3D-Digital image correlation technique. *Construction and Building Materials*, *376*(October 2022), 131061. https://doi.org/10.1016/j.conbuildmat.2023.131061
136. Xu, P., Zhou, Z., Liu, T., Pan, S., & Tan, X. (2022). In-situ damage assessment of FML joints under uniaxial tension combining with acoustic emission and DIC: Geometric influence on damage formation. *Thin-Walled Structures*, *170*(October 2021), 108515. https://doi.org/10.1016/j.tws.2021.108515
137. Yoneyama, S., & Ueda, H. (2012). Bridge deflection measurement using digital image correlation with camera movement correction. *Materials Transactions*, *53*(2), 285–290. https://doi.org/10.2320/matertrans.I-M2011843
138. Yu, L., Bekdullayev, N., & Lubineau, G. (2021). Smartphone-Based Single-Camera Stereo-DIC System: Thermal Error Analysis and Design Recommendations. *IEEE Sensors Journal*, *21*(7), 9567–9576. https://doi.org/10.1109/JSEN.2021.3054805
139. Yu, L., & Lubineau, G. (2021). A smartphone camera and built-in gyroscope based application for non-contact yet accurate off-axis structural displacement measurements. *Measurement: Journal of the International Measurement Confederation*, *167*. https://doi.org/10.1016/j.measurement.2020.108449
140. Yu, L., Tao, R., & Lubineau, G. (2019). Accurate 3D shape, displacement and deformation measurement using a Smartphone. *Sensors (Switzerland)*, *19*(3). https://doi.org/10.3390/s19030719
141. Yu, Q.-Q., & Wu, Y.-F. (2017). Fatigue Strengthening of Cracked Steel Beams with Different Configurations and Materials. *Journal of Composites for Construction*, *21*(2). https://doi.org/10.1061/(asce)cc.1943-5614.0000750
142. Zhang, N., Hedayat, A., Bolaños Sosa, H. G., Tunnah, J., González Cárdenas, J. J., & Salas Álvarez, G. E. (2021). Estimation of the mode I fracture toughness and evaluations on the strain behaviors of the compacted mine tailings from full-field displacement fields via digital image correlation. *Theoretical and Applied Fracture Mechanics*, *114*(March). https://doi.org/10.1016/j.tafmec.2021.103014
143. Zhou, K., Lei, D., He, J., Zhang, P., Bai, P., & Zhu, F. (2021). Real-time localization of micro-damage in concrete beams using DIC technology and wavelet packet analysis. *Cement and Concrete Composites*, *123*. https://doi.org/10.1016/j.cemconcomp.2021.104198
144. Ziaja, D., Turoń, B., & Miller, B. (2020). Detection of anomaly in a pretensioned bolted beam-to-column connection node using digital image correlation and neural networks. *Applied Sciences (Switzerland)*, *10*(7). https://doi.org/10.3390/app10072400
145. Zona, A. (2021). Vision-based vibration monitoring of structures and infrastructures: An overview of recent applications. *Infrastructures*, *6*(1), 1–22. https://doi.org/10.3390/INFRASTRUCTURES6010004